The dustiest Post-Main sequence stars in the Magellanic Clouds

Olivia C. Jones[1], Margaret Meixner[1,2], Benjamin A. Sargent[3], Martha L. Boyer[4,5], Marta Sewiło[6,2], Sacha Hony[7], Julia Roman-Duval[1]
ojones@stsci.edu

ABSTRACT

Using observations from the *Herschel* Inventory of The Agents of Galaxy Evolution (HERITAGE) survey of the Magellanic Clouds, we have found thirty five evolved stars and stellar end products that are bright in the far-infrared. These twenty eight (LMC) and seven (SMC) sources were selected from the 529 evolved star candidates in the HERITAGE far-infrared point source catalogs. Our source identification method is based on spectral confirmation, spectral energy distribution characteristics, careful examination of the multiwavelength images and includes constraints on the luminosity, resulting in a thoroughly vetted list of evolved stars. These sources span a wide range in luminosity and hence initial mass. We found thirteen low- to intermediate mass evolved stars, including asymptotic giant branch (AGB) stars, post-AGB stars, planetary nebulae and a symbiotic star. We also identify ten high mass stars, including four of the fifteen known B[e] stars in the Magellanic Clouds, three extreme red supergiants which are highly enshrouded by dust, a Luminous Blue Variable, a Wolf-Rayet star and two supernova remnants. Further, we report the detection of nine probable evolved objects which were previously undescribed in the literature. These sources are likely to be among the dustiest evolved objects in the Magellanic Clouds. The *Herschel* emission may either be due to dust produced by the evolved star or it may arise from swept-up ISM material.

Subject headings: stars: late-type – infrared: stars – Magellanic Clouds – circumstellar matter – stars: mass-loss - – submillimeter: stars

[1]Space Telescope Science Institute, 3700 San Martin Drive, Baltimore, MD, 21218, USA

[2]The Johns Hopkins University, Department of Physics and Astronomy, 366 Bloomberg Center, 3400 N. Charles Street, Baltimore, MD 21218, USA

[3]Center for Imaging Science and Laboratory for Multiwavelength Astrophysics, Rochester Institute of Technology, 54 Lomb Memorial Drive, Rochester, NY 14623, USA

[4]Observational Cosmology Lab, Code 665, NASA Goddard Space Flight Center, Greenbelt, MD 20771, USA

[5]Oak Ridge Associated Universities (ORAU), Oak Ridge, TN 37831, USA

[5]Space Science Institute, 4750 Walnut St. Suite 205, Boulder, CO 80301

[7]Institut für Theoretische Astrophysik, Zentrum für Astronomie, Universitt Heidelberg, Albert-Ueberle-Str. 2, D-69120 Heidelberg, Germany

1. Introduction

Evolved stars are important drivers of the chemical enrichment of the interstellar medium (ISM) of galaxies. In our own Galaxy dust enrichment of the ISM is dominated by the dusty winds from low- to intermediate mass stars (1–8 $M_{\odot}$) during the asymptotic giant branch (AGB) phase of evolution (Gehrz 1989). At lower metallicities the relative contribution from high mass stars ($M > 8M_{\odot}$) becomes important, and a significant period of dust production from these high-mass sources, via their stellar winds or directly in the supernova (SN) ejecta, is often invoked to explain the substantial dust abundances observed in high-redshift galaxies and quasars (Dwek et al. 2007; Michałowski et al. 2010; Beelen et al. 2006; Bertoldi & Cox 2002).

Dust production at low-metallicities is only

just beginning to be understood, due primarily to recent galaxy-wide surveys of nearby low metallicity systems such as the Magellanic Clouds (MC). The Large and Small Magellanic Clouds (LMC and SMC, respectively), with metallicities of 0.5 and 0.2 $Z_{\odot}$ (Russell & Dopita 1992; Tchernyshyov et al. 2015), are ideally suited to such investigations, due to their proximity (50 and 60 kpc; Ngeow & Kanbur 2008; Szewczyk et al. 2009), favorable viewing angle (35° for the LMC; van der Marel & Cioni 2001) and low average reddening along the line-of-sight ($E_{B-V} \sim 0.08$ and 0.04; Schlegel et al. 1998).

The resolved stellar populations of the Magellanic Clouds have been well studied over a wide wavelength range from the optical to the far-infrared (e.g. Zaritsky et al. 1997; Harris & Zaritsky 2004; Blum et al. 2006; Boyer et al. 2011), as these surveys cover the full spatial extent of each galaxy, a complete picture of the mass-losing stellar populations in the Magellanic Clouds can been obtained. The dust-injection rate from low-mass stars in the Magellanic Clouds has been estimated by Srinivasan et al. (2009); Matsuura et al. (2009); Riebel et al. (2012); Boyer et al. (2012), using mid-IR fluxes which are sensitive to warm ($\sim$ 100 K) dust. To compile a complete inventory of dust producers and fully characterise the stellar dust return to the ISM, the far-infrared (IR; 50–250 μm) and sub-millimeter (submm; ($\lambda \gtrsim$250 μm) emission from cold dust (T < 50 K) envelopes associated with stars in an evolved stage of stellar evolution must also be constrained.

Using data from the *Herschel* Inventory of the Agents of Galaxy Evolution in the Magellanic Clouds Open Time Key Project (HERITAGE; Meixner et al. 2013), Seale et al. (2014) created a *Herschel* band-matched source catalog (BMC) for both the LMC and SMC by combining the individual HERITAGE catalogs of point sources at 100, 160, 250, 350, and 500 μm. They classify the sources in the BMC and find that the brightest HERITAGE sources are predominately young stellar objects (YSOs) while the faintest are background galaxies. Intriguingly, they provisionally identify a smaller population ($\sim$500) of very dusty stars, in the later stages of stellar evolution (e.g. extreme AGB stars, post-AGB (PAGB) objects, planetary nebulae (PNe) and supernova remnants (SNR)), although the majority of these sources have also been identified as YSOs in other studies.

In the Milky Way, the *Herschel* Key Program MESS (Mass loss of Evolved StarS; Groenewegen et al. 2011), has observed a representative sample of low- and intermediate-mass and high-mass post-main sequence objects, across a range of mass-loss rates. They find that extended structure in the far-IR is commonly seen around AGB stars and their remnants (Kerschbaum et al. 2010; Cox et al. 2012; Maercker et al. 2012). However, the presence of a significant number of evolved stars detected in the HERITAGE survey is unexpected, as it was predicted that the majority of these sources in the Magellanic Clouds would fall below the *Herschel* sensitivity limit (Meixner et al. 2010). Only the most luminous, heavily dust enshrouded evolved stars were expected to have a detectable submm emission. The cold circumstellar envelopes of two massive evolved stars (R71 and IRAS 05280–6910) in the LMC have been detected with *Herschel* (Boyer et al. 2010). However, van Loon et al. (2010b) attribute this emission to swept-up ISM dust rather than from dust produced by the stars themselves.

The goal of this paper is to investigate the $\sim$500 evolved star candidates with a submm excess in the Magellanic Clouds identified using data from the *Herschel* HERITAGE-BMC (Seale et al. 2014). The paper is organised as follows: the observational data is summarized in Section 2. In Section 3 we describe the selection of post-main-sequence stars from the HERITAGE-BMC; in Section 4 we present the results of this search and discuss the different post-main-sequence object classes contained in the catalog. Finally, Section 5 concludes this paper.

2. Photometric Data

Far-infrared (far-IR) and submm observations of the Magellanic Clouds were taken as part of the HERITAGE Key Project (Meixner et al. 2013) using the Photodetector Array Camera and Spectrometer (PACS; Poglitsch et al. 2010) and the Spectral and Photometric Imaging Receiver (SPIRE; Griffin et al. 2010) on the *Herschel Space Observatory* (Pilbratt 2010). Photometric catalogs of point sources were created us-

ing STARFINDER (Diolaiti et al. 2000) which effectively removes diffuse emission to extract a point source flux. A full description of the HERITAGE observations and data reduction details can be found in Meixner et al. (2013).

The HERITAGE survey detected over 35000 unique sources in the LMC and 7500 in the SMC at 100, 160, 250, 350, and 500 μm. These sources were positionally cross-matched by Seale et al. (2014) to produce a HERITAGE Band-Matched catalog (BMC) for the LMC and SMC. This catalog was further matched to the *Spitzer* IRAC and MIPS catalogs from the Surveying the Agents of Galaxy Evolution (SAGE) *Spitzer* legacy surveys of the Large and Small Magellanic Clouds (Meixner et al. 2006; Gordon et al. 2011). Further details regarding the band-matching are given in Seale et al. (2014). The final HERITAGE-BMC covers the 3.6 to 500 μm range and contains over 42000 unique sources; these represent the dustiest populations of sources in the Magellanic Clouds.

In order to comprehensively classify the 500 sources in the HERITAGE photometric catalogs, and fully explore the dust production from point sources in the Magellanic Clouds, we have cross-matched the HERITAGE-BMCs with optical, near-IR and mid-IR point source catalogs, to provide photometry over a broader wavelength range (0.36 – 500 μm). The optical UBVI and near-IR JHK_s photometry comes from the Magellanic Clouds Photometric Survey (MCPS; Zaritsky et al. 1997); the Infrared Survey Facility (IRSF) Magellanic Clouds Point Source Survey (Kato et al. 2007), the Two Micron All-Sky Survey (2MASS; Skrutskie et al. 2006), and the 2MASS 6X Deep Point Source Catalog (6X2MASS; Cutri & 2MASS Team 2004). We also obtained supplementary mid-IR data from the *AKARI* LMC point source catalog (Ita et al. 2008; Kato et al. 2007) and the WISE all-sky catalog (Wright et al. 2010).

We considered sources from the various catalogs to be a match if the source is within 5″ of the IRAC 3.6 μm position in the BMC. In cases where there were multiple matches between catalogs we only considered the closest match.

To complement the photometric data we searched the spectroscopic data from the *Spitzer* SAGE-Spec survey of the Magellanic Clouds (Kemper et al. 2010; van Loon et al. 2010b) for all spectra taken with the InfraRed Spectrograph (IRS; 5.2-38 μm; Houck et al. 2004) and MIPS spectra (MIPS-SED; 52-97 μm) for matches to the HERITAGE-BMCs. We found 185 matches. These sources have been spectroscopically classified by Woods et al. (2011); Ruffle et al. (2015) and Woods et al. (in prep).

3. Refining the identification of post main sequence stars

To identify the evolved stellar population in the Magellanic Clouds with a *Herschel* detection, we compiled a preliminary candidate list from sources which were identified as dusty objects in the late stages of stellar evolution including extreme and post-AGB stars, planetary nebulae, and supernova remnants. These sources were categorized by Seale et al. (2014) by matching the HERITAGE catalogs to other classification schemes and lists of previously identified objects in the literature.

The HERITAGE BMCs contain 443 LMC and 51 SMC evolved star candidates and 45 LMC plus 9 SMC PN candidates (Seale et al. 2014). In total 455 of these Magellanic Cloud sources have also been assigned an alternate classification, making it difficult to judge the reliability of the source classifications in the initial list of evolved stars. For this reason we have to employ additional selection criteria to remove young stellar objects and background galaxies from the evolved star candidate list.

The following subsections describe our selection process, the methodology is generally listed in order of procedure however at some stages the selection criteria were assessed in parallel. For instance, an unambiguous identification can not be obtained solely upon the inspection of the source's spectral energy distribution (SED), thus the object's position and morphology was also considered simultaneously when assigning a likely classification.

3.1. Spectroscopic confirmation

The most reliable point-source classifications are obtained from spectroscopic observations. This alleviates most of the ambiguity that arises from photometric classification schemes due to overlaps in colour-magnitude space and thus provides robust source classifications for IR objects.

We compare our initial list of evolved star candidates to the SAGE-Spec spectroscopic survey of the Magellanic Clouds (Kemper et al. 2010). Of the 529 unique sources in our list, 172 were found to have a spectroscopic counterpart.

From IRS spectroscopy we find a total of seven evolved stars and four planetary nebulae. Other less-common objects were also identified; these include one blue supergiant (BSG), one B[e] star, one Luminous Blue Variable (LBV), one Wolf-Rayet (WR) star, one symbiotic star and two sources of an unknown physical nature (Woods et al. 2011; Ruffle et al. 2015, Woods et al. in prep.). Eight of these sources also have far-IR MIPS spectra covering the 52–97μm wavelength range (van Loon et al. 2010b,a). The remaining 154 objects with an IRS counterpart were confirmed spectroscopically as YSOs or HII regions (Woods et al. 2011; Oliveira et al. 2013; Ruffle et al. 2015). We remove these sources from the list of the evolved star candidates. The results of the spectral comparisons are summarised in Tables 1 and 2.

From the IRS spectra we have identified 18 post main sequence stars. Spectroscopic confirmation is still needed for the majority ($\sim$ 60%) of the BMC evolved star candidates. For these 357 sources, we use several other complementary metrics in parallel to find evolved objects, improve upon the source identification and to exclude non-evolved contaminants from our sample.

3.2. SED classification

Photometrically it can be difficult to separate AGB stars from YSOs and young PNe from compact HII regions. The colour selection criteria for the far-IR sources from Boyer et al. (2011) and the candidate post-AGB stars from van Aarle et al. (2011) heavily overlap with the same regions as the YSO candidates in the colour magnitude diagrams (CMD). As such many of these sources have multiple classifications in the literature and we expect a high degree of contamination from YSOs in our initial evolved star sample selection.

To refine our selection further, the nature of each object with a far-IR detection was assessed by examining its SED from near-IR to far-IR wavelengths. Figure 1 shows some illustrative examples of typical SEDs for the different classes of objects. Based on the shape of the SED with the flux plotted in $\log(\lambda F_\lambda)$ against $\log(\lambda)$ and more specifically on the peak of the energy distribution we can (tentatively) divide the sources in our list into four separate classes: (1) evolved star candidate, (2) probable YSO, (3) possible background galaxy, (4) a mismatch between the near- and far-IR data used in this study.

3.2.1. Evolved star candidates

The most extreme AGB stars can have red colours similar to YSOs, background galaxies, and PNe, and will also display a rising SED between 8 to 24 μm. We identify dust enshrouded AGB stars based on the peak of the SED; dusty AGB stars typically peak in the IRAC bands (<8 μm), while stars with little to no circumstellar dust peak in the near-IR. As the AGB star becomes more obscured the peak of the SED shifts to longer wavelengths, and the SED may peak between 8 and 24 μm for the most extreme AGB stars. AGB stars detected with *Herschel* will fall in the latter category due to the cool dust envelopes which are likely providing additional extinction at the shorter wavelengths. In all cases the shape of the SED for AGB stars resembles that of a blackbody with temperature between 100 and 3000 K.

Red supergiants are more massive and are in general more luminous than AGB stars. As they exhibit a similar dust chemistry to oxygen-rich AGB stars, their SEDs are virtually indistinguishable. Ancillary information such as luminosity, pulsation period or membership of a young cluster is generally required to separate these classes (see Section 3.4).

Post-AGB stars tend to have a double-peaked SED, with one peak in the optical/near-IR (due to a hot central stellar component) and one in the mid-IR (due to a detached shell of circumstellar emission). This double-peaked morphology enables one to readily distinguish post-AGB stars from SEDs with a stellar component which has a large infrared excess.

The SEDs of other more massive evolved stars such as LBVs, WR stars and BSGs tend to be double-peaked, showing a stellar photosphere and a strong far-infrared excess. The classifications for these sources are taken from the literature (e.g. Bonanos et al. 2009, 2010), and are not solely

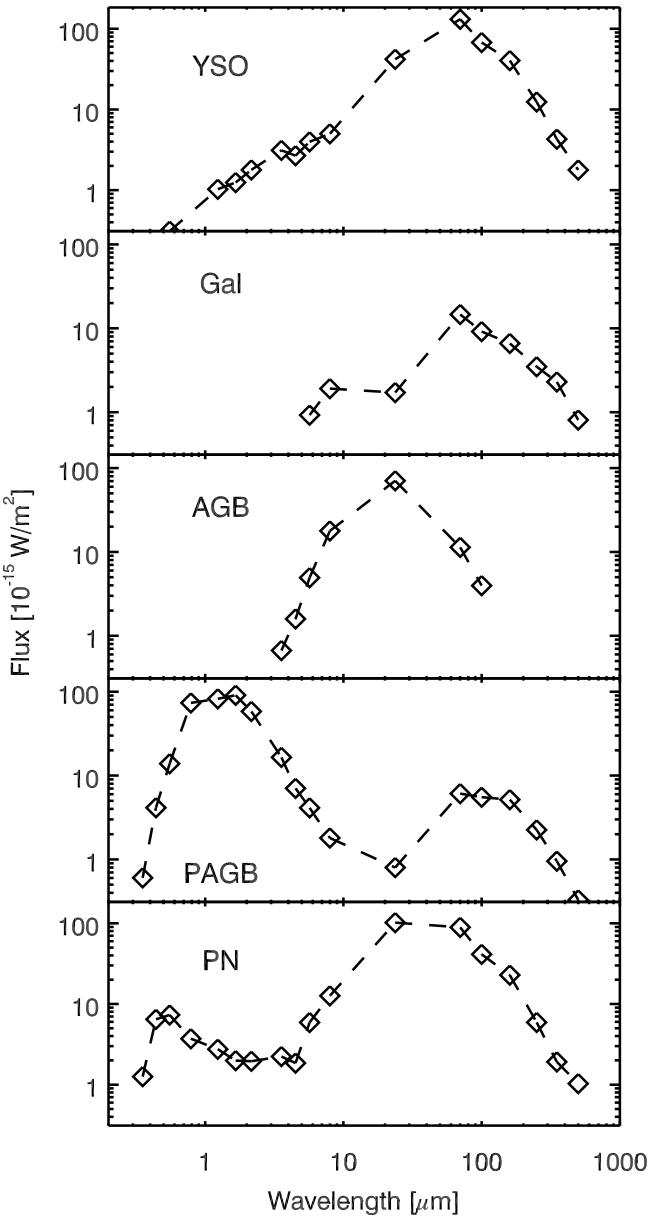

Fig. 1.— Example SEDs for the different groups of objects, including a YSO, a background galaxy, an AGB star with a large dust excess, a double-peaked SED indicative of a PAGB star, and a PN. The shape of the SED for YSOs differs markedly from the evolved stars.

based on the SED.

3.2.2. YSO candidates

The SEDs of Stage 0/I YSOs (early to mid-stage YSOs) show a monotonic increase from the mid-IR to the far-IR, with the peak at ∼100 μm. Objects which peak in the far-IR are heavily obscured by cold dust, which absorbs the photospheric emission from the forming star, and re-radiates this energy at far-IR wavelengths. As the YSO evolves it dissipates its surroundings and emission from warm dust begins to dominate the SED. For stars in the latest stages of formation, the peak emission is blue-ward of the far-IR, and these objects can be difficult to disentangle from other sources with a warm circumstellar dust continuum (Oliveira et al. 2009). Given the high likelihood of contamination from YSOs in our sample, additional care needs to be taken when inspecting the shape and peak of the energy distribution for these objects. However, objects which have an SED peak between 70 and 150 μm are likely YSOs (e.g. Sewiło et al. 2013).

To break the degeneracy between YSOs in the more advanced stage of formation and evolved stars which exhibit a significant IR excess, we created a mean YSO SED for each evolutionary stage based on the 154 YSOs with a spectroscopic counterpart (see Woods et al. 2011, for each YSO spectral class). These YSOs range from Stage 0/1–4 and cover a wide range in luminosity. Using the YSO SED templates as a basis, we only retained those objects which peaked at wavelengths $< 70\mu$m or had a significantly different profile to that of a YSO. We find 197 evolved star candidates closely mimic the SEDs of the previously identified YSOs. After their removal, our sample contains 178 dusty evolved star candidates.

3.2.3. PNe & background galaxies

The SEDs of PNe have a very similar appearance to those of YSOs, both in terms of shape and in the position of the peak; rising from the mid-IR and peaking in the far-IR. Background galaxies also tend to have a rising SED in the mid-IR, and the peak of their SEDs tends to lie in the *Herschel* bands. We can not resort to SEDs to distinguish between these classes. We further consider potential confusion with background galaxies in

Section 3.3.2.

3.2.4. Misclassification and mismatches

At low flux levels where a source is only detected in a few *Herschel* bands, the shape of the SED can be difficult to characterize. This can also be problematic in crowded fields, such as star-forming regions where there is a high probability of misidentification between photometric catalogs, due to the wide range in resolution between the surveys. We examine the SEDs for any large discontinuities between the photometry from different instruments and point source catalogs, indicative of a likely mismatch. An example of a mismatch between the photometric catalogs is shown in the bottom panel of Figure 2. The SEDs for these sources are most likely a combination of a point source with warm circumstellar dust and spatially coincident starless dust clump which radiated in the far-IR. We eliminate 109 BMC evolved star candidates from the sample due to a discontinuity in the SED.

Low flux levels may also be problematic when comparing sources in the HERITAGE-BMC to objects previously identified in the literature, as this leads to higher positional uncertainties. This positional uncertainty in turn results in the potential misclassification of the BMC source as an evolved star. It is therefore vital that any source identified in the HERITAGE-BMC as an evolved star has a smooth SED with data points that appear consistent with each other and are associated with a point source.

3.2.5. SEDs of the final candidate list

Figures 3 and 7 show the SEDs (as well as the available spectral data) for the final candidate list of post main-sequence objects in the MCs. In all instances a smooth transition is seen between the 2MASS, *Spitzer* and *Herschel* photometry, thus the shapes of the SEDs in the IR are well defined. At shorter wavelengths it is sometimes unclear if the MCPS data is associated with the source due to the difference in resolution, the high circumstellar extinction at optical wavelengths and intrinsic variability of the source.

The SEDs show a range of distinguishing features due to the presence of warm and cold dust, which is dependent on the mass-loss history of the

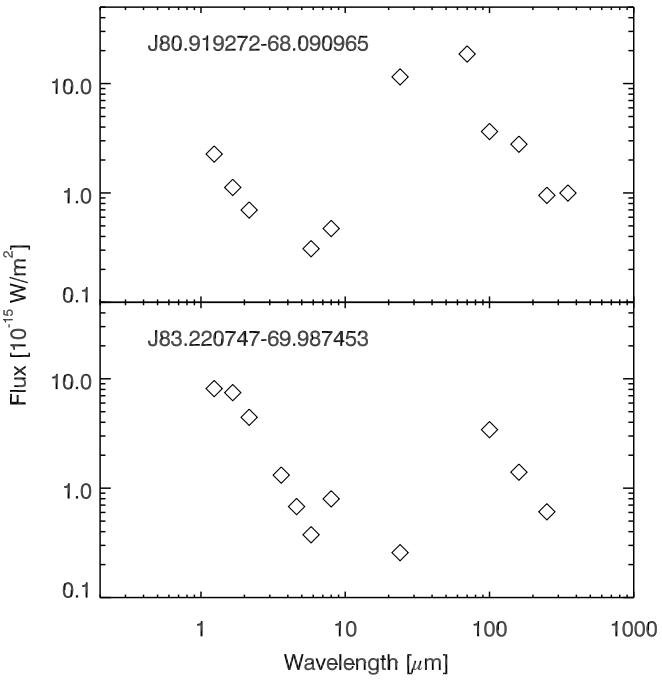

Fig. 2.— An example SED for a source in the BMC which is similar in appearance to that of a YSO (top) and for a source where there is a mismatch between the *Herschel* flux and the photometric data at shorter wavelengths (bottom).

source. In all instances the SEDs are consistent with post main-sequence stars; the final classification is noted in each panel.

3.3. Image inspection

Using multiwavelength observations we assess the nature of each source in our initial sample. In several instances a source may only be identified in one or two *Herschel* bands and may be missing counterparts at other wavelengths. Simutanious inspection of the images and the SEDs ensures that the BMC sources are real and not a composite of several nearby sources which contribute to the emission at different wavelengths, resulting from a mismatch between the *Herschel* and *Spitzer* catalogs.

The PACS images are known to suffer from low level artifacts (in the form of striping and cross-hatching) (Meixner et al. 2013) which may affect the quality and reliability of point sources extracted from the original images at 100 and 160μm. Thus care needs to be taken when studying compact objects detected in the PACS bands.

In an effort to obtain high-quality PACS images at 100 and 160μm, the HERITAGE PACS data have been reprocessed with the Tamasis[1] software (Chanal and Panuzzo, private communication) which mitigates thermal drifts in the PACS imaging using the redundancy and high pass filtering of the observations, effectively removing the artificial structures that compromised the original images. However, the Tamasis images cannot be used to extract photometry because the mapping technique and filtering makes the photometry potentially systematically inaccurate. Thus, we must inspect the refined PACS Tamasis images to distinguish between striping and point-sources in the HERITAGE BMC. We remove three spurious sources that are only detected with PACS and are coincident with the striped/hashed regions in the original images.

3.3.1. Evolved stars vs. YSOs

To determine the likelihood that a given source is an evolved star we conduct a careful visual inspection of the IRAC, MIPS, PACS and SPIRE images. Magellanic Cloud Emission Line

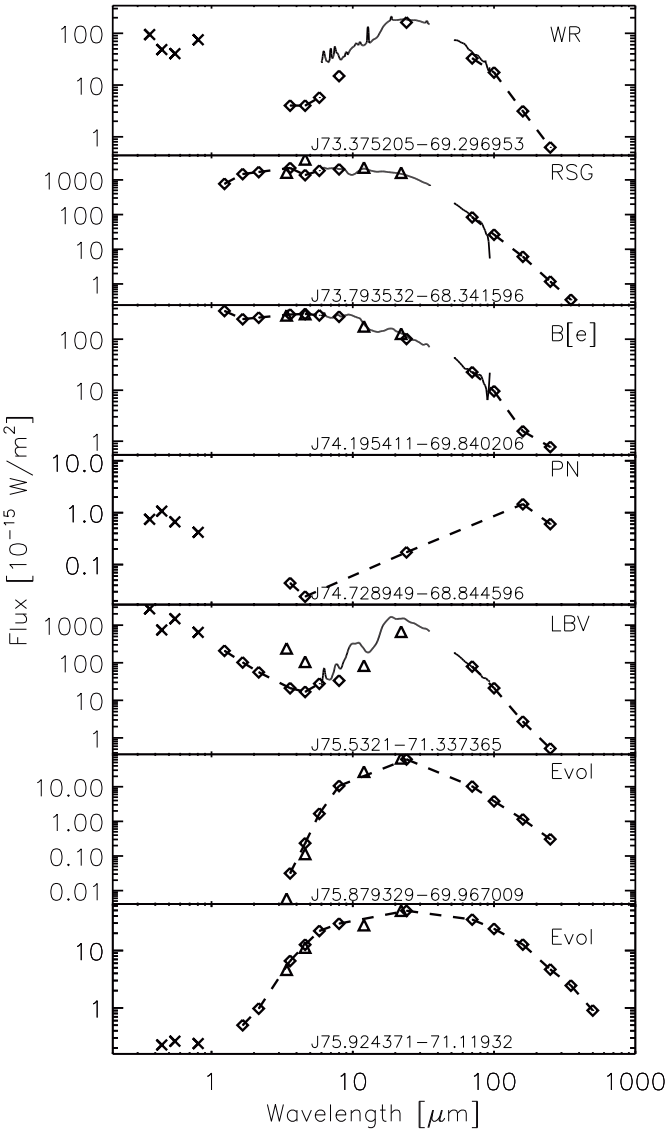

Fig. 3.— SEDs and spectra for the post-main sequence sources in the LMC, ordered in terms of RA. Data from the HERITAGE-BMC and SAGE catalogs are shown as the dashed-diamond line, MCPS data as crosses, WISE data as triangles and AKARI data as squares.

[1] http://pchanial.github.io/tamasis-pacs/

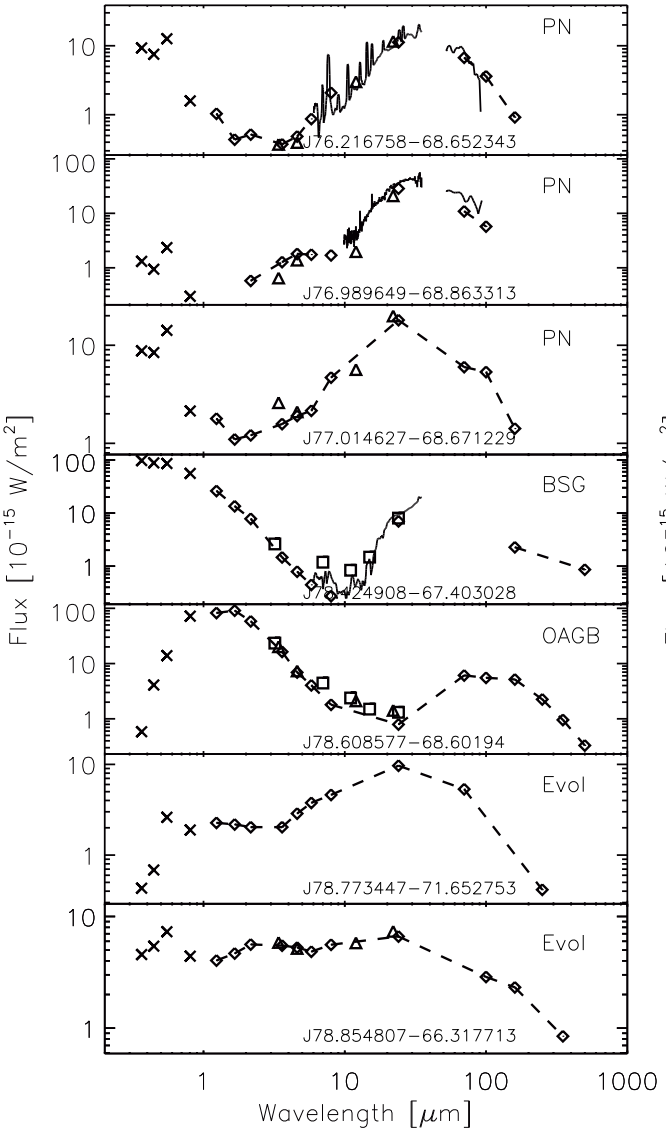

Fig. 4.— Fig. 3. Continued.

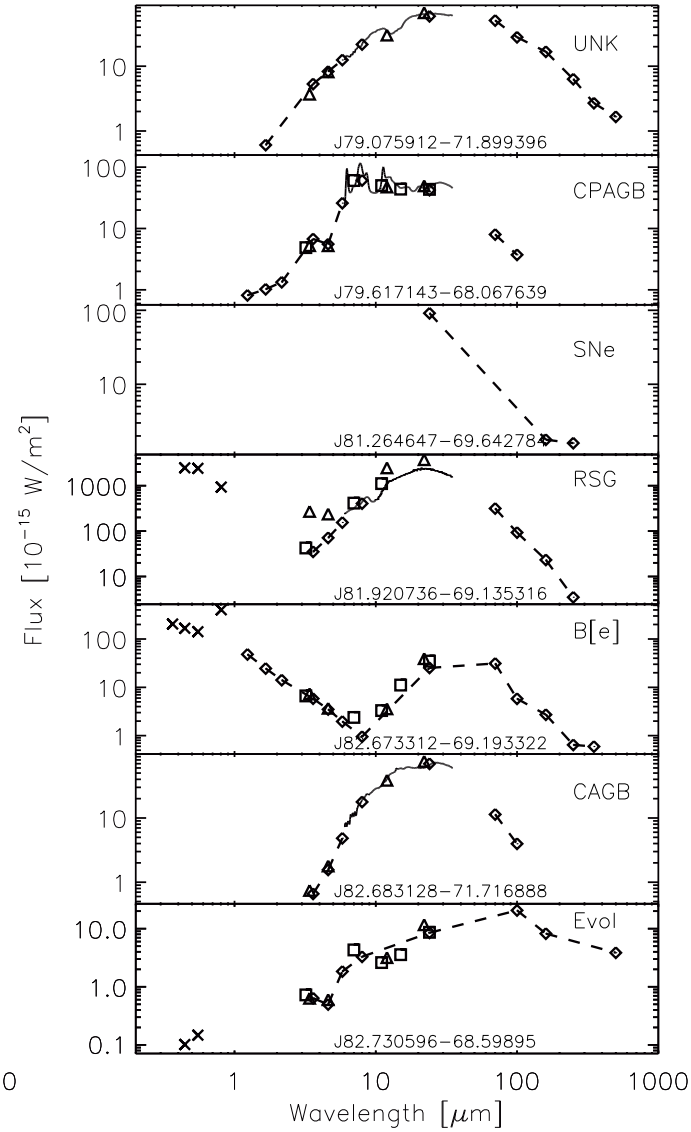

Fig. 5.— Fig. 3. Continued.

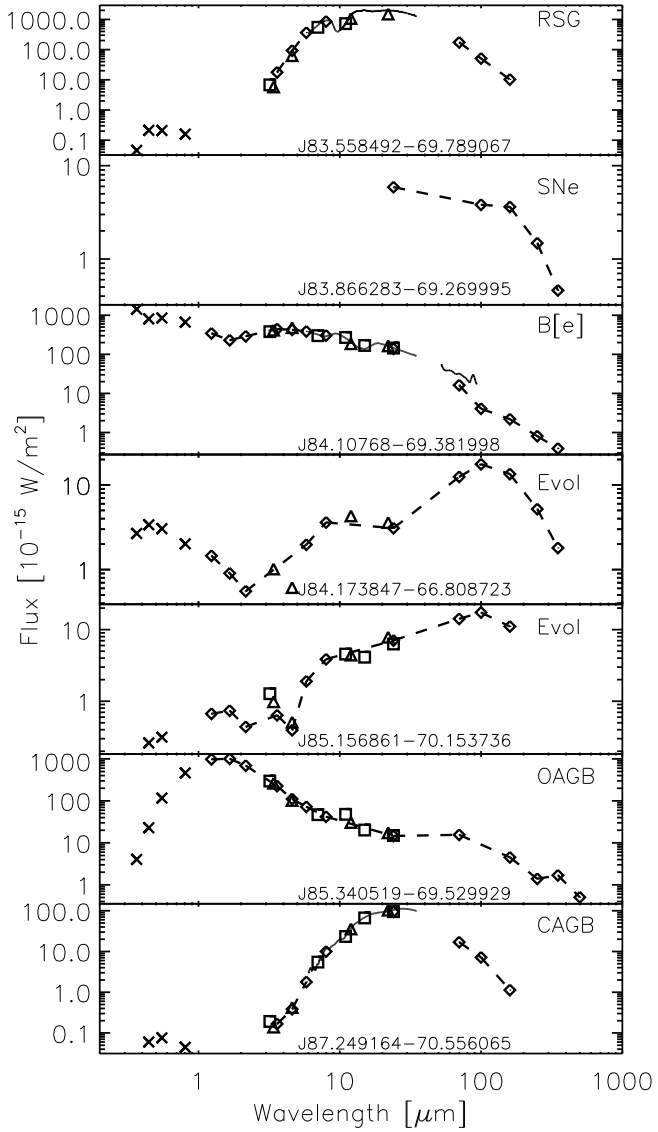

Fig. 6.— Fig. 3. Continued.

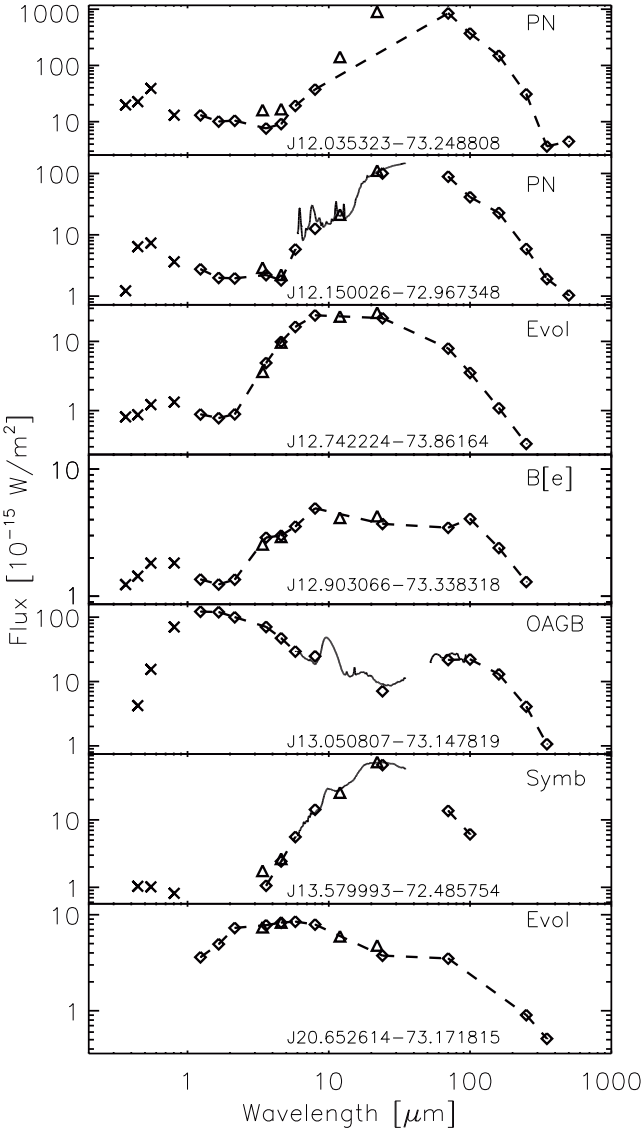

Fig. 7.— As for Fig. 3, but now for the SMC.

Survey (MCELS; Smith & MCELS Team 1998) Hα images were also examined. Using DS9 (Joye & Mandel 2003) we simultaneously view each evolved star candidate across multiple wavelengths, facilitating the inspection of the local stellar and interstellar environment.

YSOs and dust clumps tend to be concentrated along bright ISM filaments (Kim et al. 2010; Sewiło et al. 2013); conversely, we expect there to be very few AGB stars associated with interstellar gas or dust structures. Evolved stars are generally isolated and inhabit regions of low column density. Inspection of the images indicates that many of the HERITAGE-BMC evolved star candidates are embedded within bright knots of emission, located along large-scale dusty ISM structures, or are concentrated around molecular clouds; suggesting that these evolved star candidates are instead likely to be YSOs or massive stars. We remove sources located within sites of massive star formation from our list if their SED also resembles that of a YSO.

Visual inspection of the *Spitzer* images reveal a cluster-like morphology at the location of several of our evolved star candidates. This morphology is typical of small proto clusters, which appear as a single massive object in *Herschel*. The spatial resolution of the HERITAGE images is > 2 pc at the distance of the Magellanic Clouds, and blending of clustered sources is prevalent. The BMC contains a GroupID which specifies group membership and is assigned to sources that have multiple matches in the BMC. As the majority of the sources in the catalog are not sorted into groups we use this criterion as an additional indication of evolutionary status and ensure that only isolated sources are retained.

3.3.2. Background galaxies/AGN

Some nearby galaxies are resolved with *Spitzer* IRAC and can be identified from their morphology; for one source in particular (HSOBMHERICC J85.622736-71.433709) we see a clear spiral pattern in the image. Other galaxies (e.g. HSOBMHERICC J82.644586-68.104609) appear elongated and have an edge-on disc morphology, we remove fifteen spatially resolved galaxies from the sample.

As a secondary diagnostic for background galaxies, Seale et al. (2014) identified distant galaxies in the BMC via their shape in the SPIRE images. Distant galaxies will be isolated from interstellar gas and dust structures, and appear unresolved and thus point-like at the *Herschel* wavelengths. Whereas, other HERITAGE source's, such as YSOs and dust clumps will appear slightly extended at SPIRE wavelengths. For each source in the BMC, Seale et al. (2014) compares the sources 250 μm full-width half-maximum (FWHM) to that of the point spread function (PSF). If the values are consistent to within 10%, the source is defined to be point-like. Twenty eight sources in our sample fulfill this criterion, although not all of them are necessarily background galaxies. Evolved stars without a detached shell will also appear point-like, thus we regard the shape in the far-IR as a rather weak constraint for separating background galaxies from AGB stars in the Magellanic Clouds, and do not remove any object on this basis.

3.4. Luminosity checks

To further refine our evolved star candidate list, we calculate the bolometric luminosity of the sources via a trapezoidal integration of the SED, from the optical to the far-IR (e.g. Woods et al. 2011; Jones et al. 2014; Ruffle et al. 2015). All sources within each Magellanic Cloud are considered to be at approximately the same distance and we use a distance modulus of 18.5 to the LMC and 18.9 to the SMC (Keller & Wood 2006). Where possible, we also compute luminosities using the IRSF photometry rather than the 2MASS data and fold in the photometry from the WISE and AKARI surveys.

Figure 8 shows the absolute bolometric magnitudes distribution of the evolved star candidates in the LMC and SMC. The luminosites for the majority of the objects in our sample are consistent with evolved stars. Objects more luminous than the classical AGB luminosity limit of $M_{\rm bol} = -7.1$ (Wood et al. 1983) may be RSGs or massive AGB stars undergoing hot bottom burning. At the low-luminosity end objects with $M_{\rm bol} > -3.9$ will be fainter than the tip of the Red Giant Branch (RGB) and are unlikely to be an evolved star, as stars on the RGB or early AGB do not experience significant dust formation. In general these limits are not an absolute division between the RGB, AGB and RSG classes, instead they provide useful

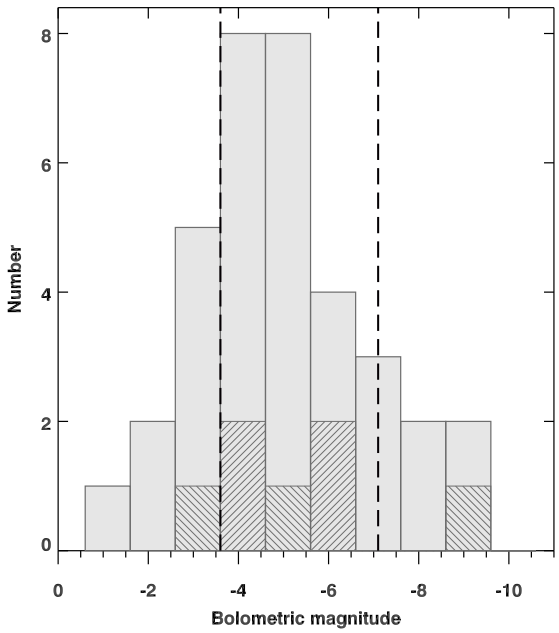

Fig. 8.— The luminosity distribution of the evolved star candidates in the LMC (solid grey) and SMC (black-striped). The dashed lines mark the expected luminosity range of AGB stars.

guidance on the likely class.

3.5. Literature classification

To aid in the final classification, we performed a SIMBAD[2] search on all of the sources to retrieve any other information pertinent to the classification. We found that twelve of our sources are relatively unknown in the literature, 26 are identified as evolved stars or PNe with a high degree of confidence and 5 were classified as a YSO (see Section 4). We removed known early type stars from our list if they were identified by means other than colour-magnitude cuts.

3.6. YSO-fitter screen

Finally we fit the evolved star candidates using the Robitaille et al. (2006, 2007) grid of YSO models, and visually examine the SED and model fits. We define well-fitted models as those whose χ^2 per data point is less than ten.

The YSO-fitter has been shown to be a good method of separating evolved stars from YSO candidates, since the YSO models do not span the high luminosities and relatively cool photospheres typical of evolved stars (Whitney et al. 2008). For other populations such as PNe the YSO fitter is less effective as a discriminant, as YSOs and PNe have similar SEDs and colours. For these sources a good fit does not inevitably imply that the source is a YSO. For the evolved star candidates 3 of the 38 sources were well fit by the YSO models; these sources are more likely to be true YSOs than a post-main sequence star, and thus they are removed from the sample.

4. Results

4.1. Classification Summary

From the 529 evolved stars candidates provisionally identified in the HERITAGE BMCs, we find strong evidence for 35 post main sequence stars. Eighteen of these sources were confirmed spectroscopically while the remaining seventeen sources were selected using the stringent criteria described in Section 3. In total 206 objects were rejected from our initial BMC sample as their SEDs and location suggests these are YSOs; a

[2]http://simbad.u-strasbg.fr/simbad/

small number (< 17) of these sources may potentially be evolved.

Tables 1 and 2 list our final catalog of evolved stars, PNe and SNR with a *Herschel* detection in the LMC and SMC, respectively; their spatial distribution on the sky is displayed in Figure 9, overlaid upon the HERITAGE 250 μm images of the LMC and SMC.

Figures 3 and 7 present the SEDs spanning optical to far-IR wavelengths of each object in the sample, and the photometry used to construct the SEDs is summarized in Table 3. Finally, Table 4 provides a tally of the various classes of post main sequence stars in the HERITAGE BMC. The following subsections discuss the individual objects in our final sample grouped according to their initial mass and evolutionary status.

4.2. Comparisons to colour-magnitude diagrams

IR colour-magnitude diagrams have been used to classify large numbers of objects detected by photometric surveys in the MCs (e.g. Blum et al. 2006; Matsuura et al. 2009; Boyer et al. 2011). We compare the evolved sources with a *Herschel* detection to mid-IR colour-magnitude diagrams of the total evolved stellar population of the LMC and SMC. Figure 10 shows the objects identified as candidate evolved stars detected with *Herschel* plotted as blue diamonds in the [8.0] versus [3.6]–[8.0] CMD; Figure 11 shows them in the [24] versus [8.0]–[24] diagram. The stars in our sample tend to be offset/isolated from the majority of evolved star candidates identified from the SAGE sample; they are much redder in colour and have bright [8] and [24] magnitudes. Due to their very dusty nature they typically lie outside CMD cuts for evolved stars or reside in areas of high confusion.

In the LMC there are four exceptions to this. These sources are identified as HSOBMHERICC J78.424908-67.403028 (BSDL 923), J78.608577-68.60194 (2MASS J05142617–6836085), J82.673312-69.193322 (HV 2605) and J85.340519-69.529929 (HV 5999) and are classified as either O-AGB/PAGB stars or blue supergiants. These stars are oxygen-rich and have SEDs that show a hot stellar component and a second peak at longer wavelengths due to a detached dust shell. Thus their [3.6]–[8.0] colour will resemble an evolved star with little

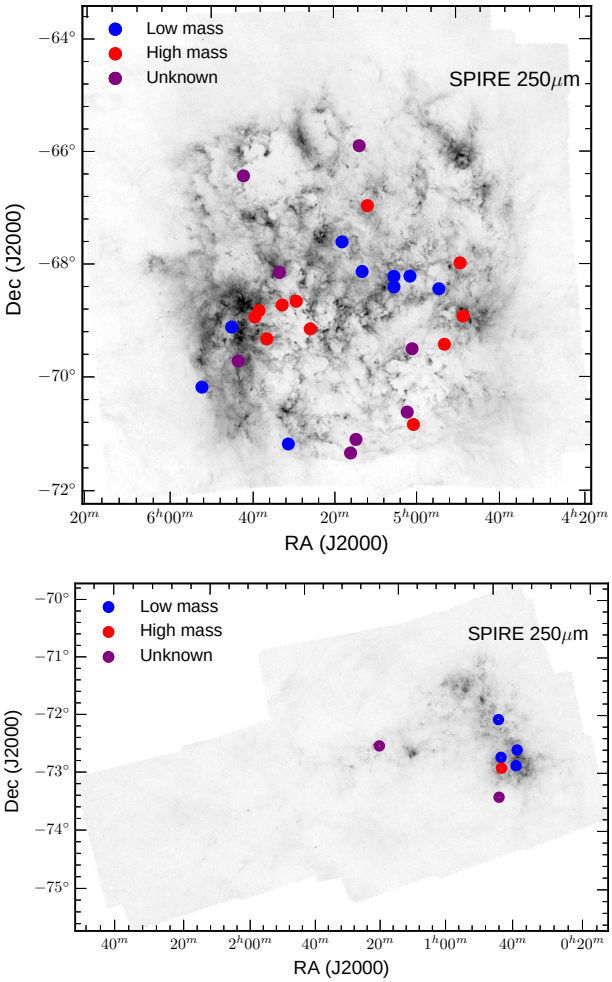

Fig. 9.— The BMC post-main sequence sources distributed on the sky, overlaid upon the HERITAGE SPIRE 250 μm images of the LMC (top) and SMC (bottom).

Table 1: Details of the final sample of evolved star candidates in the LMC. For each source, the BMC name, BMC coordinates, bolometric magnitudes ($M_{\rm bol}$), total luminosity, SAGE-Spec identification (SSID) and final classification is given (see Section 4 for details).

BMC Source Name	Alias	RA (J2000)	Decl. (J2000)	$M_{\rm bol}$	Luminosity ($L_\odot$)	SSID	Classification
J73.375205-69.296953	Brey 3a	04:53:30.0	−69:17:49	−5.9	17784	4060	WR
J73.793532-68.341596	WOH G064	04:55:10.4	−68:20:30	−9.3	403277	4091	RSG
J74.195411-69.840206	R66	04:56:46.9	−69:50:25	−7.1	52908	4113	B[e]
J74.728949-68.844596	RP 1805	04:58:54.9	−68:50:41	−1.5	331	24	PN
J75.5321-71.337365	R71	05:02:07.0	−71:20:13	−7.1	55722	4162	LBV
J75.879329-69.967009	...	05:03:31.0	−69:58:01	−4.8	6668	...	Possible evol.
J75.924371-71.11932	...	05:03:41.8	−71:07:10	−5.2	9874	...	Possible evol.
J76.216758-68.652343	SMP LMC 21	05:04:52.0	−68:39:08	−3.3	1715	4196	OPN
J76.989649-68.863313	SMP LMC 28	05:07:57.5	−68:51:48	−4.1	3518	4209	OPN
J77.014627-68.671229	SMP LMC 29	05:08:03.5	−68:40:16	−3.8	2516	...	PN
J78.424908-67.403028	BSDL 923	05:13:41.9	−67:24:11	−3.5	1913	69	BSG
J78.608577-68.60194	...	05:14:26.0	−68:36:07	−4.6	5374	...	O-AGB/PAGB
J78.773447-71.652753	...	05:15:05.6	−71:39:10	−3.4	1776	...	Possible evol.
J78.854807-66.317713	...	05:15:25.0	−66:19:04	−3.4	1825	...	Possible evol.
J79.075912-71.899396	IRAS 05170–7156	05:16:18.2	−71:53:58	−5.4	11702	78	UNK
J79.617143-68.067639	IRAS 05185–6806	05:18:28.1	−68:04:04	−4.9	7201	4307	C-PAGB
J81.264647-69.642784	N 132D	05:25:02.0	−69:38:39	...	...	...	SNR
J81.920736-69.135316	IRAS 05280–6910	05:27:46.2	−69:08:07	−7.8	107347	4454	RSG
J82.673312-69.193322	[BE74] 328	05:30:41.5	−69:11:36	−4.7	6224	...	B[e]
J82.683128-71.716888	IRAS 05315–7145	05:30:43.9	−71:43:01	−5.0	7688	125	C-AGB
J82.730596-68.59895	...	05:30:55.3	−68:35:56	−4.2	3938	...	Possible evol.
J83.558492-69.789067	IRAS 05346–6949	05:34:14.0	−69:47:21	−7.7	91262	4555	RSG
J83.866283-69.269995	SN 1987A	05:35:28.0	−69:16:11	...	...	...	SNR
J84.10768-69.381998	R126	05:36:25.8	−69:22:55	−7.3	64377	4601	B[e]
J84.173847-66.808723	...	05:36:42.0	−66:48:31	−3.8	2529	...	Possible evol.
J85.156861-70.153736	...	05:40:37.6	−70:09:13	−3.8	2543	...	Possible evol.
J85.340519-69.529929	HN 5999	05:41:21.7	−69:31:48	−7.1	56957	...	O-AGB
J87.249164-70.556065	IRAS 05495–7034	05:48:59.7	−70:33:22	−5.3	10049	190	C-AGB

Note: The HERITAGE-BMC designation prefix is HSOBMHERICC.

Table 2: Details of the final sample of evolved star candidates in the SMC. For each source, the BMC name, alias, BMC coordinates, bolometric magnitudes ($M_{\rm bol}$), total luminosity, SMC IRS identification (SMC IRS) and final classification is given.

BMC Source Name	Alias	RA (J2000)	Decl. (J2000)	$M_{\rm bol}$	Luminosity ($L_\odot$)	SMC IRS	Classification
J12.035323-73.248808	LIN 107	00:48:08.5	−73:14:56	−9.0	324932	...	PN
J12.150026-72.967348	LIN 115	00:48:36.0	−72:58:02	−6.2	24197	32	CPN
J12.742224-73.86164	...	00:50:58.1	−73:51:42	−4.6	5427	...	Possible evol.
J12.903066-73.338318	Jacoby SMC 17	00:51:36.7	−73:20:18	−3.3	1624	...	B[e]
J13.050807-73.147819	BMB-B 75	00:52:12.2	−73:08:52	−5.9	17561	177	O-AGB
J13.579993-72.485754	...	00:54:19.0	−72:29:09	−5.2	9946	260	Symbiotic star
J20.652614-73.171815	...	01:22:36.6	−73:10:19	−3.7	2404	...	Possible evol.

Note: The HERITAGE-BMC designation prefix is HSOBMHERICC.

Table 3: Summary of the columns present in the table of photometry which is available on-line only.

Column Number	Column Name	Description	Null Value
1	SourceName	HERITAGE-BMC Designation	...
2	RA	Right Ascension (J2000)	...
3	Dec	Declination (J2000)	...
4	Galaxy	LMC or SMC	...
5-12	fU, dU, fB,dB, fV, dV, fI, dI	MCPS U, B, V, I fluxes (f) and errors (d) [mJy]	-999.9
13-18	fJ, dJ, fH, dH, fK, dK	2MASS J, H, K fluxes and errors [mJy]	-999.9
19-26	f3.6, d3.6, f4.5, d4.5, f5.8, d5.8, f8.0, d8.0	IRAC fluxes and errors [mJy]	-999.9
27-30	f24, d24, f70, d70	MIPS fluxes and errors [mJy]	-999.9
31-40	f100, d100, f160, d160, f250, d250, f350, d350, f500, d500	PACS & SPIRE fluxes and errors [mJy]	-999.9
41-45	flag100, flag160, flag250, flag350, flag500	HERITAGE-BMC quality flags	-999.9
46-53	fW1, dW1, W2, dW2, fW3, dW3, fW4, dW4	WISE flux and errors [mJy]	-999.9
54-63	fN3, dN3, fS7, dS7, fS11, dfS11, fL15, dfL15, fL22, dfL22	AKARI flux and errors [mJy]	-999.9
64	SSID/ SMC IRS	Spectral Identification number of the target from Woods et al. (2011); Ruffle et al. (2015) and Woods et al. (in prep).	-999.9

Table 4: Classification groups and tally for the LMC and SMC.

LMC		SMC	
Type	Count	Type	Count
B[e]	3	B[e]	1
BSG	1	O-AGB	1
C-AGB	2	PN	2
C-PAGB	1	Possible evol.	2
LBV	1	Symbiotic star	1
O-AGB	1		
O-AGB/PAGB	1		
PN	4		
Possible evol.	7		
RSG	3		
SNR	2		
UNK	1		
WR	1		
Total	28	Total	7

circumstellar excess, while at [8.0]–[24] the contribution from circumstellar dust becomes significant and their colours resemble the other stars in our sample with a strong dust excess.

4.3. Low and intermediate mass stars

Our sample contains thirteen confirmed low to intermediate mass stars and PNe, which make up 32 per cent of the total sample. If we include the possible evolved stars (Section 4.6), which have unknown mass, this value could rise to 60 per cent of the probable evolved sources detected in the HERITAGE-BMC. Due to their intrinsic brightness, stars with masses below $8M_{\odot}$ were not expected to be recovered by the HERITAGE survey, as only dust ejected by a few of the most massive stars were predicted to have luminosities greater than the *Herschel* sensitivity limits.

The intermediate mass stars we detect include two of the most extreme AGB stars in the LMC with exceptionally high mass-loss rates, whose carbon rich chemistry has been confirmed spectroscopically (Gruendl et al. 2008). The SEDs of the two carbon stars (C-AGB) and the symbiotic (AGB-white dwarf binary) star do not show any evidence for excess emission in the far-IR, however. All the oxygen-rich AGB (O-AGB) stars in our sample show a stellar component, a component due to warm dust and in some instances a far-IR excess may also be present. This excess may be associated with the dust-driven wind, a stable circumstellar disc or dust swept-up from the surrounding ISM. The mass-loss rate stated for the

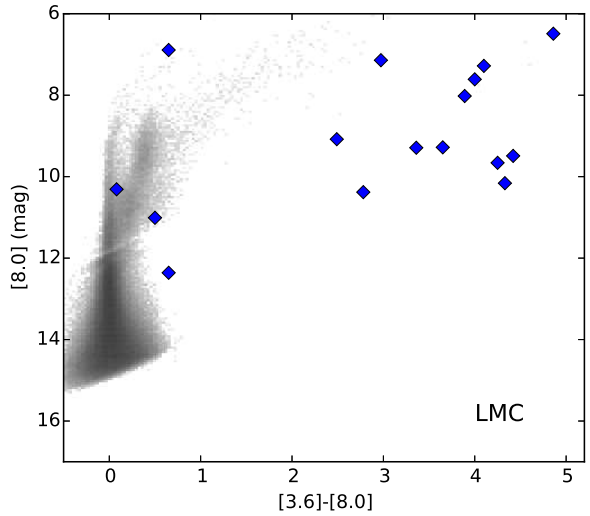

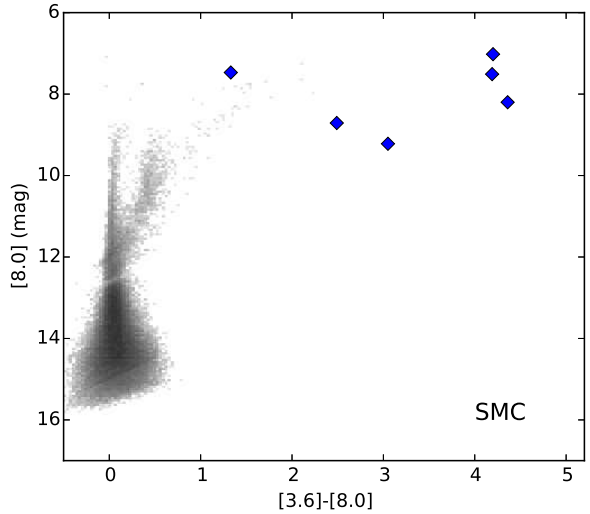

Fig. 10.— The [8.0] vs. [3.6]–[8.0] CMD for the LMC (top) and SMC (bottom) showing the distribution of the post-main sequence stars in our final sample (blue diamonds) plotted over a Hess diagram of the evolved star sample of Boyer et al. (2011) for the LMC and SMC.

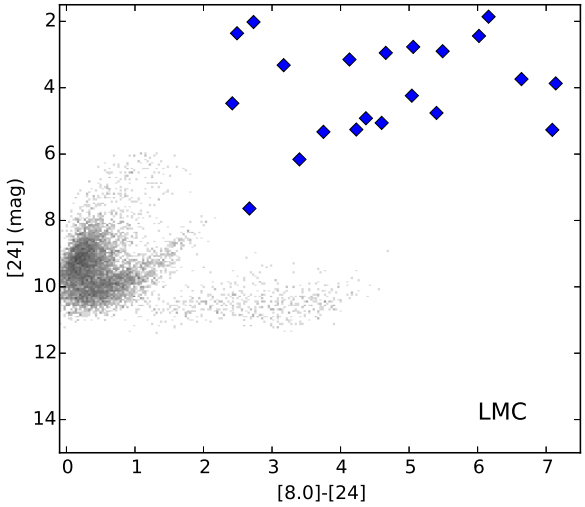

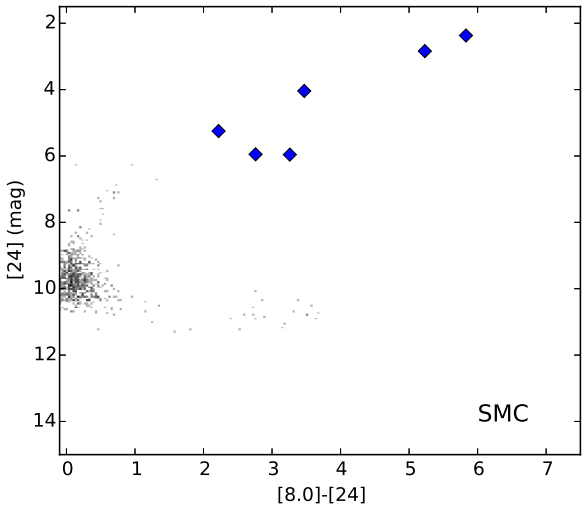

Fig. 11.— The [24] vs. [8.0]–[24] CMD for the LMC (top) and SMC (bottom) showing the distribution of the post-main sequence stars in our final sample (blue diamonds) plotted over a Hess diagram of the evolved star sample of Boyer et al. (2011) for the LMC and SMC.

O-AGB stars is likely an underestimate as current model grids do not account for complex dust geometries due to a detached shell. Detailed 3D radiative-transfer modeling of the sources with a far-IR excess is required to determine reliable dust production rates and to differentiate between ISM dust and dust produced in the stellar wind (Jones et al., in preparation, Paper II).

Our final sample also includes several highly evolved post-superwind objects such as planetary nebulae. The five planetary nebulae in our sample have been identified from a combination of Hα images, optical ionized gas emission lines and mid-IR spectra. Due to the similarities between the SEDs of PNe and YSOs and the strict criteria we applied when selecting the evolved star sample it is likely that we have excluded some PNe from our final list. Thus the number of PNe with a *Herschel* counterpart included in our final catalog should be treated as a lower limit.

4.3.1. AGB stars

HSOBMHERICC J78.608577-68.60194 (2MASS J05142617–6836085): This long period variable (P = 382 d; Fraser et al. 2008) is likely oxygen-rich. It was found to have a mass-loss rate (MLR) of 2.8×10^{-7} $M_{\odot}\,yr^{-1}$ (Riebel et al. 2012). The SED is double peaked which may indicate that the source is a post-AGB star or that it has an unresolved detached shell.

HSOBMHERICC J82.683128-71.716888 (IRAS 05315–7145) is an extreme carbon-rich AGB star, heavily obscured by dust. It has a very high mass-loss rate of 1.7×10^{-4} $M_{\odot}\,yr^{-1}$ (Gruendl et al. 2008); this is the second highest of all the extreme AGB (x-AGB) stars in the LMC. SiC absorption features are present in the IRS spectra.

HSOBMHERICC J85.340519-69.529929 (HV 5999): This source has a luminosity of $M_{\rm bol} = -7.1$ mag and a spectral type of M3 suggesting the source is likely a massive O-rich AGB star undergoing hot bottom burning or is a red supergiant. It is also included in the RSG catalog of Massey & Olsen (2003), who give $M_{\rm bol} = -8.05$ mag. Fits with GRAMS indicate that this source is oxygen-rich with a mass-loss rate of 1.4×10^{-6} $M_{\odot}\,yr^{-1}$ (Riebel et al. 2012). The SED shows evidence of a far-IR excess which (if associated with the star) may indicate the presence of large (μm – mm size) grains and/or cold dust in a detached shell.

HSOBMHERICC J87.249164-70.556065 (IRAS 05495–7034) is an extremely red carbon star first identified by Gruendl et al. (2008). Its spectra show the presence of amorphous carbon, SiC absorption features, and a strong MgS feature at 30 μm. This 'extremely red object' (ERO) has the highest mass-loss rate (2.3×10^{-4} $M_{\odot}\,yr^{-1}$) of all the x-AGB stars in the LMC (Gruendl et al. 2008).

HSOBMHERICC J13.050807-73.147819 (BMB-B 75) is a Mira-type variable with a long period of P = 1453 d (Cioni & Habing 2003). It is an M6-type star (Blanco et al. 1980). The star is oxygen-rich with a mass-loss rate of 1.5×10^{-5} $M_{\odot}\,yr^{-1}$ (Jones et al. 2012). Recently a redshifted galaxy (z$\sim$0.16) has been discovered in the same line of sight as BMB-B 75 (Kraemer et al. 2015, in prep.) The far-IR emission detected by *Herschel* is probably due to this spatially coincident galaxy.

HSOBMHERICC J13.579993-72.485754 (SSTISAGEMA J005419.21-722909.7) is a D-type symbiotic star, consisting of an AGB star and white dwarf (Oliveira et al. 2013). Of the seven known symbiotic stars in the SMC it is the only one with warm dust; this dust is silicate rich and unprocessed as it shows no PAH emission.

4.3.2. Post-AGB stars

Our sample only includes one confirmed post-AGB star. However Seale et al. (2014) notes that the BMC contains four confirmed post-AGB stars from van Aarle et al. (2011) with low resolution optical spectra. Of these four sources, both HSOBMHERICC J73.375205-69.296953 and J78.854807-66.317713 are included in our sample as a WR star and a probable evolved star, respectively (see Sections 4.4 and 4.6). However, HSOBMHERICC J80.919272-68.090965 and J83.220747-69.987453 were eliminated from our sample either because the SED resembles that of a YSO or because the SED at longer wavelengths appears disjointed and the *Herschel* data were attributed to a mismatch. The SEDs of these two sources are shown in Figure 2.

HSOBMHERICC J79.617143-68.067639 (IRAS 05185–6806) was first identified as a likely post-AGB object by van Loon et al. (1997). Its mid-

IR *Spitzer*-IRS spectrum shows the presence of the unidentified 21-μm feature found only in carbon-rich post-AGB stars (Volk et al. 2011; Matsuura et al. 2014; Sloan et al. 2014), confirming that mass loss during the AGB phase has terminated.

4.3.3. PNe

HSOBMHERICC J76.216758-68.652343 (SMP LMC 21) is a very high-excitation, quadrupolar PN of Type I (Stanghellini et al. 1999). It has an extremely strong IR-excess ($T_{dust\,cont}$ = 130 K) and the *Spitzer* IR spectrum shows prominent crystalline silicate emission due to forsterite and enstatite. No other solid-state features are seen (Stanghellini et al. 2007). The spectrum also shows both low and very high excitation nebular emission lines (i.e., [S III] and [Ne VI], respectively). It is one of the reddest PNe in the Magellanic Clouds. The ionized mass in the nebula is determined to be between 0.2 – 0.6 $M_\odot$ (Barlow 1987; Boffi & Stanghellini 1994), and the progenitor is thought to be a relatively massive AGB star.

HSOBMHERICC J76.989649-68.863313 (SMP LMC 28) is a high-excitation, isolated, oxygen-rich PN (Reid & Parker 2006; Hora et al. 2008; Bernard-Salas et al. 2009). It is has a high nitrogen and neon abundance compared to other PNe (Stanghellini et al. 2005; Bernard-Salas et al. 2008). This PN is resolved in HST images and has three co-aligned round shapes, corresponding to the central star and two faint arms (Shaw et al. 2001). The central star was detected by Villaver et al. (2003). They estimate its luminosity to be $L = 1.4 \times 10^4 L_\odot$, with $T_{eff} \lesssim 17000$ K, which corresponds to a progenitor mass of $\sim 3M_\odot$. The ionized mass in the nebula is $< 0.2M_\odot$ (Wood et al. 1987).

HSOBMHERICC J77.014627-68.671229 (LHA 120-N 102/ SMP LMC 29) is a bright PN noted to have strong emission lines (Reid & Parker 2006). This PN is resolved and has an irregular shape with a bipolar core in HST images. It is thought to be one of the smallest bipolar PNe recognised to date, with radius of ∼0.27 arcsec in [O III] (Shaw et al. 2006). No central star is evident within the bright nebulosity of the image (Villaver et al. 2003). It has emission lines in high states of ionization (e.g., N V) which have extreme photoionization temperatures (T ∼ 200 kK) (Herald & Bianchi 2007).

HSOBMHERICC J12.150026-72.967348 (Lin 115/ SMP SMC 11) is a well known carbon-rich PN which was first discovered by Henize (1956). Both emission line observations and PAH features in its IRS spectrum confirm its carbon-rich nature (Stanghellini et al. 2003; Bernard-Salas et al. 2009). High-resolution HST images show that it has a complex bipolar morphology, which extends out to 2″ from the center (Stanghellini et al. 2003). It has strong mid-IR emission; the dust continuum sharply rises after 12 μm and its SED peaks around 35 μm, indicative of a far-IR-excess (Bernard-Salas et al. 2009).

HSOBMHERICC J12.035323-73.248808 (LIN 107) was identified as a planetary nebula by Lindsay (1961); Meyssonnier & Azzopardi (1993). Other authors list this object as a weak emission-line object or 'low-excitation blob' (Meynadier & Heydari-Malayeri 2007; Sheets et al. 2013; Testor et al. 2014) suggesting that it is an embedded star cluster or compact HII region.

4.4. Massive stars

We have compared the HERITAGE-BMC to the *Spitzer* catalogs of massive stars in the Magellanic Clouds (Bonanos et al. 2009, 2010) and find nine matches in the LMC and one match in the SMC. This is approximately twice the number anticipated prior to the HERITAGE observations. Notably far-IR emission is observed for four of the fifteen confirmed B[e] stars in the Magellanic Clouds, while only one of the 106 late-type WR stars has a far-IR detection.

Three heavily dust enshrouded extreme RSGs are also detected. These stars all optically thick in the mid-IR where amorphous silicate absorption features are seen at 10 and (in some instances) 20 μm indicative of extremely high mass-loss rates, which may be as large as 10^{-3} $M_\odot$ yr^{-1} (Dijkstra et al. 2003). The mass loss from these three sources was missed in dust budget estimates for the LMC by Riebel et al. (2012).

4.4.1. BSG stars

HSOBMHERICC J78.424908-67.403028 (BSDL 923) is a blue supergiant (BSG); a massive star, newly evolved from the main sequence. Its loca-

tion in the young cluster LMC-N30 (Gouliermis et al. 2003; Bica et al. 1999) is consistent with that of a massive star. The SED is distinctly double-peaked, falling to a minimum at ∼8 μm before rising steeply long-ward of 15 μm; this red peak is due to a circumstellar disc or torus. Weak silicate features are seen in its *Spitzer*-IRS spectrum (Woods et al. 2011).

4.4.2. RSG stars

HSOBMHERICC J73.793532-68.341596 (WOH G064) is a very luminous red supergiant with spectral type M7.5 (Elias et al. 1986) and an effective temperature of $T_{\rm eff} \sim 3200$ K. It is surrounded by a thick dust shell and is one of six evolved stars in the Magellanic Clouds to have a 10 μm amorphous silicate feature in self-absorption (Roche et al. 1993; Trams et al. 1999; Buchanan et al. 2006; Kemper et al. 2010, Jones et al. (in prep)). Its mass-loss rate is estimated to be in the region of 10^{-3} $M_\odot\,{\rm yr}^{-1}$ (van Loon et al. 2005a) with a wind speed of $v_{\rm wind} \sim 25{\rm kms}^{-1}$, determined from OH, SiO, and H_2O maser emission (Wood et al. 1986; van Loon et al. 1996, 1998; Marshall et al. 2004). The circumstellar dust shell was resolved by Ohnaka et al. (2008), who found that the envelope had a bipolar geometry; they derived a circumstellar envelope mass of 3–9 $M_\odot$.

We estimate the bolometric luminosity to be 4×10^5 $L_\odot$ ($M_{\rm bol} = -9.3$), however if the geometry of the dust shell is non spherical then the bolometric luminosity is an overestimate. Accounting for the non spherical nature of the shell Ohnaka et al. (2008) determine the luminosity to be 2.8×10^5 $L_\odot$ ($M_{\rm bol} = -8.8$) leading to a down-ward revision of the star's initial mass to $M_{\rm ZAMS} \sim 25M_\odot$. Its location beyond the Hayashi limit in the H-R diagram indicates that the star is no longer in hydrostatic equilibrium (Levesque et al. 2007) and it may be experiencing an intense unstable phase of heavy mass loss. van Loon et al. (2010b) suggests that the mass-loss rate of WOH G064 has increased dramatically in the past few thousand years (i.e. it has experienced the onset of the superwind phase), as they find no evidence for a submm excess.

HSOBMHERICC J81.920736-69.135316 (IRAS 05280–6910) is a highly obscured OH/IR red supergiant with an initial mass $M_{\rm ZAMS} \sim 20M_\odot$ (Wood et al. 1992). Its stellar counterpart was identified using high-resolution near- and mid-IR imagery by van Loon et al. (2005b). OH maser emission has been used to determine its wind outflow velocity which is $\approx 20{\rm kms}^{-1}$ (Marshall et al. 2004); the star also exhibits H_2O maser emission (van Loon et al. 2001). It has an extremely high mass-loss rate of $\dot{M} \simeq 2 - 8 \times 10^{-3}$ $M_\odot\,{\rm yr}^{-1}$ (Boyer et al. 2010) and is potentially the most dust-enshrouded supergiant in the Magellanic Clouds. In the IRS spectra both the 10 and 20 μm amorphous silicate features are seen in absorption and a declining, featureless continuum is seen at far-IR wavelengths (Kemper et al. 2010). The dust shell may have a flattened geometry which (unlike WOH G064) is viewed edge-on. The total dust mass is ≈ 0.3 $M_\odot$. There is no evidence of excess emission at $\lambda > 100$ μm, implying that there is no significant contribution from dust colder than ∼100 K or from large (μm - mm size) grains in a detached shell (van Loon et al. 2010b; Boyer et al. 2010).

HSOBMHERICC J83.558492-69.789067 (IRAS 05346-6949): This luminous oxygen-rich red supergiant is highly obscured (Elias et al. 1986); due to its very red IRAC [3.6]–[4.5] ∼ 2.5 colour it has been classified as an ERO by Gruendl & Chu (2009) and an extreme-AGB star by Srinivasan et al. (2009). We classify it as a RSG because of its high luminosity and the silicate features present in its IRS spectrum (Jones et al. 2014). Unlike many sources in the ERO class this source is not carbon-rich, instead it has an oxygen-rich dust composition. Like WOH G064, the *Spitzer*-IRS spectrum of *HSOBMHERICC J83.558492-69.789067* exhibits a 10 μm silicate feature in absorption (Jones et al. 2012, Woods et al. (in prep), Jones et al. (in prep)) which means that the dust envelope is optically thick, and the star is experiencing heavy mass loss. Despite being bright in the mid-IR, any maser emission has not been detected (van Loon et al. 2001) and the source is not bright in the optical. Radio continuum emission at 1420 MHz may be associated with the source.

4.4.3. B[e] stars

HSOBMHERICC J74.195411-69.840206 (R66) is a well-known B[e] supergiant of spectral type B8 Ia, with luminosity $L = 3 \times 10^5$, $T_{\rm eff} \sim 12000$ K and an initial mass of $M_{\rm ZAMS} \sim 30M_\odot$ (Lamers et al. 1998; Stahl et al. 1983). The

star is both cool and below the Humphreys-Davidson limit (Zickgraf et al. 1986), leading van Loon et al. (2010b) to suggest that it is a blue-loop star on its way back to becoming an RSG. The *Spitzer*-IRS spectrum shows PAHs, amorphous silicates and strong crystalline silicate features, indicative of dust grain processing in a long-lived pole-on circumstellar disc (Kastner et al. 2006, 2010; Aret et al. 2012). This disc is massive and contains $\approx 0.001\ M_{\odot}$ of dust.

HSOBMHERICC J82.673312-69.193322 ([BE74] 328) is a luminous ($M_{\rm bol} = -10.15$; Massey 2002), emission line star of spectral type B1.5IIe (Reid & Parker 2012). It is listed as a poorly studied eruptive variable of early spectral type in the General catalog of Variable Stars (Samus et al. 2004).

HSOBMHERICC J84.10768-69.381998 (R126) is an extremely luminous B[e] supergiant in the LMC. Its bolometric luminosity is $L = 1.2 \times 10^6 {\rm L}_{\odot}$, with ${\rm T}_{\rm eff} \sim 22500$ K and is estimated to have an initial mass of ${\rm M}_{\rm ZAMS} \sim 75 {\rm M}_{\odot}$. Its present day mass is ${\rm M} \sim 40 {\rm M}_{\odot}$ (Zickgraf et al. 1985). Estimates for the current mass-loss rate range between $\dot{M} = 10^{-6} - 4.6 \times 10^{-5}\ M_{\odot}$ yr^{-1}, depending on the assumed terminal velocity of the stellar wind $v_{\infty} \approx 650 - 1800$ km s^{-1} (Zickgraf et al. 1985; Bjorkman et al. 1998). R 126 is thought to have a relatively massive 'puffed up' circumstellar disc which is estimated to contain ${\rm M}_{\rm dust} \approx 0.003\ {\rm M}_{\odot}$ of dust (Kastner et al. 2006). Detailed analysis of R 126's disc can be found in Porter (2003); Kraus et al. (2007).

HSOBMHERICC J12.903066-73.338318 (Jacoby SMC 17) is included in the list of probable B[e] supergiants in the SMC (Mennickent et al. 2002), as its light curve resembles Galactic B[e] stars. Meyssonnier & Azzopardi (1993) identify the source as a very low excitation object with a blue continuum. It was also identified as an emission line star by Murphy & Bessell (2000). It may potentially be a PN (Boroson & Liebert 1989); its total luminosity is on the low-side for a B[e] star but is consistent with a PNe.

4.4.4. LBV stars

HSOBMHERICC J75.5321-71.337365 (R71) is one of six confirmed dusty luminous blue variables (LBVs) in the LMC (Humphreys & Davidson 1994). Its initial mass is estimated to be ${\rm M}_{\rm ZAMS} \sim 40 {\rm M}_{\odot}$ (Lennon et al. 1993). LBVs can develop instabilities and show sudden bursts of mass loss; this mass-loss history can be probed via dusty ring nebulae often associated with the star (Hutsemekers 1994). R71 recently experienced an eruption, where there was a $\sim$2 mag increase in the V-band brightness (Szczygieł et al. 2010). This increase in emission is not seen in our mid-IR data which show a smooth transition between the *Spitzer* and *Herschel* photometry, even-though the *Herschel* data were obtained post-eruption, while the *Spitzer* observations were obtained prior to the outburst. The difference in flux between the *WISE* bands at 3.4 and 4.6 μm and the IRAC bands may be due to the increased emission from the photosphere during the recent outburst.

The dust shell of R 71 contains PAHs, and both amorphous and crystalline silicates indicative of non-equilibrium chemistry. It estimated to contain 0.02 ${\rm M}_{\odot}$ of dust, ejected at a rate of 7×10^{-6} ${\rm M}_{\odot}\,{\rm yr}^{-1}$ over the past 3000 years. A second dust shell from an earlier expulsion event is estimated to contain 0.3 ${\rm M}_{\odot}$ of dust (Voors et al. 1999). This second dust shell has been called in to question by van Loon et al. (2010b) and Guha Niyogi et al. (2014) who find that R 71 lacks dust colder than $T_{\rm d} \lesssim 100$ K.

Using data from the HERITAGE Science Demonstration Program Boyer et al. (2010) measured a far-IR dust component at $\lambda > 250$ μm. In later HERITAGE photometric data-sets, which better accounts for background emission, the SPIRE 350 and 500 μm is confirmed to be diffuse. Using this refined photometry, Guha Niyogi et al. (2014) have fit radiative transfer models to R71 and derive a total dust mass of 0.01 ${\rm M}_{\odot}$ and a time-averaged dust mass-loss rate of 2.5×10^{-6} ${\rm M}_{\odot}\,{\rm yr}^{-1}$.

4.4.5. WR stars

HSOBMHERICC J73.375205-69.296953 (Brey 3a/ BAT99-4) is a WC9-type Wolf-Rayet (WR) star with a progenitor mass believed to be in excess of 25 ${\rm M}_{\odot}$ (Breysacher et al. 1999). Late-type WR stars can lose mass at rates of up to 10^{-4} ${\rm M}_{\odot}\,{\rm yr}^{-1}$ (Crowther 2007). Characterised by strong He, N and C emission lines and red SEDs due to warm circumstellar dust, WR stars are relatively easy to identify; there are thought

to be 134 WR stars in the LMC. Brey 3a is unusual as its exact spectral type remains controversial, leading some authors to dispute its WR status and instead suggest that it may be a transition object between an Of star and a WR star (Moffat 1991; Heydari-Malayeri & Melnick 1992). Egan et al. (2001) note the presence of an M3-type red giant 5.2″ away from Brey 3a, which may contribute some flux at <24 μm but van Loon et al. (2010b) find that the far-IR emission seen in the MIPS-SED spectra of Brey 3a is typical of a WR-type star rather than an M-type giant with warm circumstellar dust. The IRS spectrum, which rises steeply at ∼15 μm, also resembles that of the WR-type star (Woods et al. 2011).

4.5. Supernova remnants

Our *Herschel* sample includes two well known supernova remnants:

A detailed analysis of SN 1987A *(HSOBMHERICC J83.866283-69.269995)* in the far-IR/sub-mm was conducted by Matsuura et al. (2011, 2015); Indebetouw et al. (2014), who found that the SN ejecta contained a large reservoir of freshly-synthesised cold dust grains with a temperature of ∼20 K and a dust mass of 0.4–0.8 $M_\odot$. This dust mass (measured 24 years after the explosion) is significantly higher than the $10^{-4}M_\odot$ of dust reported in the first couple of years following the explosion (Wooden et al. 1993); providing the first clear evidence that supernovae can produce significant amounts of dust and that they can be an important source of dust in the ISM of galaxies. The dust produced in the ejecta is thought to be composed of silicates and amorphous carbon. As the core-collapse SN is rapidly evolving and the expanding ejecta have yet to interact with the warm (∼170 K) circumstellar dust ring (ejected from its red supergiant progenitor; Barkat & Wheeler 1988) and experience reverse shocks which may potentially destroy or alter the grains (e.g., Jones et al. 1994; Lakićević et al. 2015; Temim et al. 2015), the total quantity of dust ejected into the ISM by SNe remains uncertain.

HSOBMHERICC J81.264647-69.642784 (N 132D) is the remnant of a core-collapse supernova that exploded ∼2700 years ago (Williams et al. 2006). The supernova remnant was detected as a slightly extended point source in two *Herschel* bands. Unlike SN 1987A, the emission from N 132D at these wavelengths is too faint to accurately constrain the dust mass of the ejecta. N132D is one of the brightest X-ray remnants in the Magellanic Clouds, and its extended emission has been extensively studied in optical and IR wavelengths (Morse et al. 1995); the bright mid-IR emission has been attributed to swept-up ISM dust collisionally heated by the hot X-ray emitting plasma generated by SN blast waves (Williams et al. 2006). *Spitzer* observations also reveal large polycyclic aromatic hydrocarbons (PAHs) that have been processed by thermal sputtering in the blast wave (Tappe et al. 2006). Dust created in the SN ejecta has been observed by Rho et al. (2009), via IR spectral lines; they estimate the mass of the newly formed dust in the ejecta to be >0.008 $M_\odot$.

The far-IR emission from other Magellanic Cloud supernova remnants (see Otsuka et al. 2010; Lakićević et al. 2015, and references therein) are not included in the HERITAGE point source catalogs as the dust emission from these remnants is either too faint or it is extended and large enough to be resolved by the *Herschel* observations.

4.6. Possible evolved stars

Two sources in our sample have low signal-to-noise or very unusual/unidentifiable features in the corresponding *Spitzer*-IRS spectra. Due to this uncertainty Woods et al. (2011) classified these sources as unknown objects. As the true nature of these objects has not been spectroscopically confirmed, we assign these objects a possible evolved star status.

HSOBMHERICC J74.728949-68.844596 is probably a planetary nebula (RP 1805); it has a diameter in Hα of 5 arcsec (Reid & Parker 2006). The mid-IR IRS-spectrum of the source shows no clear identifying features above the noise and was thus reported as a non-detection. The source is faint and appears elongated the SAGE-LMC 8-μm images. A UV-bright star located within 1 arcmin of the source could conceivably be irradiating the dust cloud.

HSOBMHERICC J79.075912-71.899396 (IRAS 05170-7156) is an unusual object. It was assigned an unknown (UKN) spectral type by Woods et al. (2011). The mid-IR spectrum rises

toward longer wavelengths and is featureless apart from a dip in the continuum between 11.5–16.0 μm. Its SED is indicative of a post-main sequence object, however, it has also been considered to be an AGN candidate (de Grijp et al. 1987; Kozłowski & Kochanek 2009) and a high-probability Stage 1 YSO (Whitney et al. 2008).

Nine sources in our sample are relatively unstudied in the literature, but detailed examination of the SEDs and fits with YSO models suggest that these sources are likely evolved stars. Only one source HSOBMHERICC J84.173847-66.808723 was given a less certain classification due to its unusual multi-peaked SED and other characteristics which meant that an alternate classification could not conclusively be ruled out.

4.7. Physical extent of dust shells

Bow shocks due to wind-ISM interactions and detached shells around AGB stars are commonly seen in the Milky Way via their far-IR excess emission (Kerschbaum et al. 2010; Groenewegen et al. 2011; Cox et al. 2012). High-mass evolved stars are often associated with a ring nebula formed from either past stellar eruptions or by swept up ISM material. In all instances the maximum physical size observed between the central star and the detached shell or bow shock is smaller than 1 pc (Cox et al. 2012). These size scales are much smaller than the highest achievable resolution of 8.6–8.8″, 2–3 pc at 100 μm in the HERITAGE images.

Given the physical size of the *Herschel* beam, we cannot use the images to distinguish between dust formed in the ejecta or dust swept-up from the surrounding ISM. Instead, the spectral energy distributions may provide some indication of far-infrared excess emission. The circumstellar envelopes of the extreme carbon stars, RSGs, LBV and WR stars in our sample lack a far-IR excess, and thus are unlikely to have large (μm – mm size) grains or harbor any significant reservoirs of cold dust. However, we may see excess emission (i.e. above what is expected from a circumstellar shell) from some of the oxygen-rich evolved stars, planetary nebulae and B[e] supergiants. This emission may either be due to dust produced by the evolved star or it may arise from swept-up ISM material.

Dust mass estimates obtained using graybody fits to the far-IR emission can in principle be used to identify the likely source of this emission (e.g. Seale et al. 2014), however this method is unlikely to yield reliable dust masses due to the complex geometry of the objects in our sample. Instead 3D radiative transfer modeling is required to derive reliable dust masses and temperatures (Jones et al. in prep, Paper II). High-resolution follow-up observations with the Atacama Large Millimeter/submillimeter Array (ALMA) should also uncover the true source of this far-IR emission. Followup observations will probe the mass-loss rate history of the star or the wind-ISM interaction at low metallicity.

4.8. Selection effects and completeness

The evolved stars in our sample were identified from the HERITAGE far-IR BMC, as such they are subject to the same biases, selection effects and limitation discussed in detail by Seale et al. (2014). Notably, the HERITAGE SPIRE observations are more sensitive than the PACS observations, thus faint sources near the sensitivity limit are detected only at 250 and 350 μm. This will adversely affect the detection of evolved stars which are expected to be brighter in the PACS bands compared to SPIRE.

In the HERITAGE images complex structures of knots and filaments due to ISM dust dominate the background emission; this prevents the detection of faint sources in regions of high background. While AGB stars are unlikely to be directly associated with dust clumps or filaments, many may lie along the same line of sight. This is even more problematic for massive stars which are preferentially found in higher ISM column densities. High background ($B_{250} > 10$ MJy sr^{-1}) regions cover 16% of the LMC and 2% of the SMC; in these regions the BMC is complete for sources brighter than 200 mJy (Seale et al. 2014). This is a factor of two greater than the completeness limits in low surface brightness regions. If our sample is distributed evenly across the Magellanic Clouds, then bright extended emission in the Magellanic Clouds may mask around five bona fide evolved stars with far-IR emission greater than 100 mJy. If we also take into account sources in the BMC which may potentially be evolved but were not included in our final list (as they are more likely to be YSOs) then this estimate increases to approxi-

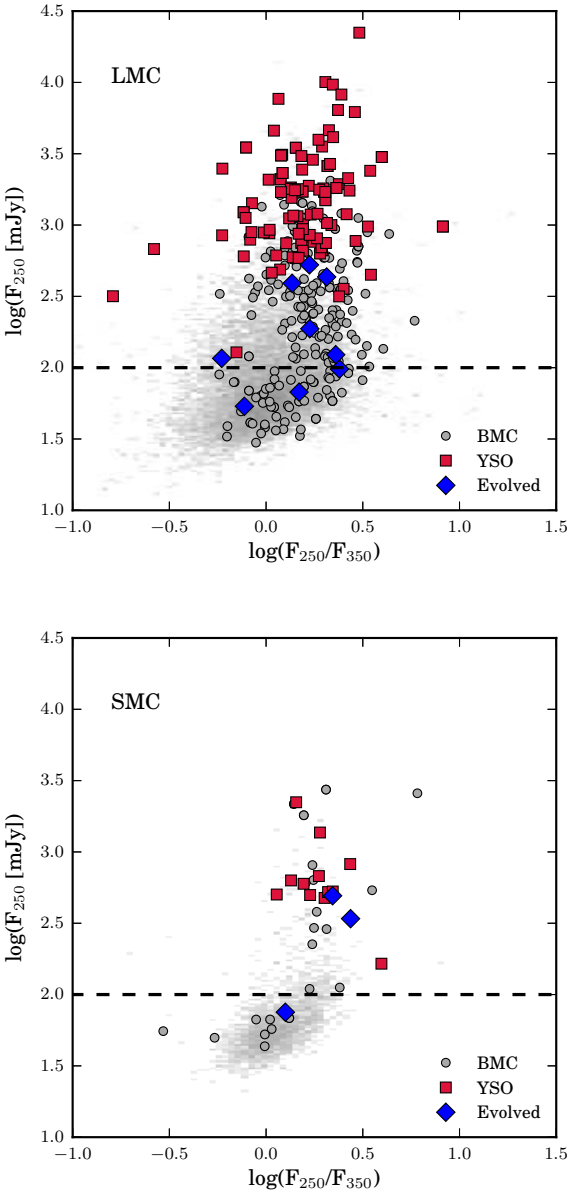

Fig. 12.— SPIRE F_{250} and F_{350} CMD for the confirmed evolved sources (blue) in the LMC (top) and SMC (bottom) overlaid on a Hess diagram of the HERITAGE Band-Matched Catalog sources. The grey circles represent the initial list of BMC candidate evolved stars and the red squares show the candidate evolved stars which have been confirmed spectroscopically as YSOs. The dashed line marks the completeness limit of the BMC at low backgrounds.

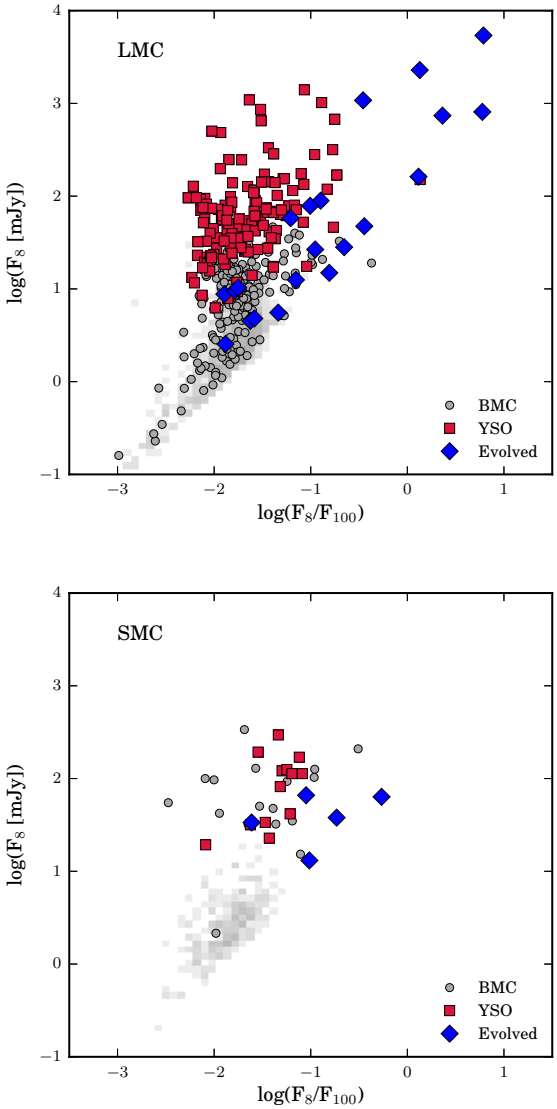

Fig. 13.— IRAC F_8 and PACS F_{100} CMD. Description as in Figure 12.

mately 10 sources. The Magellanic Clouds should therefore host between 18 and 23 post-main sequence stars with far-IR fluxes greater than the BMC completeness limit, rather than the 13 we currently detect. The remaining 22 sources in our sample are faint and fall below this limit; here we do not have enough statistical information to provide a quantitative value for the total population of faint evolved stars with similar fluxes.

The identification of evolved stars in the BMC is biased towards brighter sources; these are prominent above the background and have an SED which is well sampled. To be included in our final list of probable evolved stars, each object must also be detected as a point-source in the mid-IR and be previously identified as an evolved star candidate in the literature or via photometric colour cuts. As such we do not discover any new objects in our vetted sample. Faint sources which are variable and optically bright (e.g. OGLE variable stars), but have a low mid-IR flux will be excluded from our list as they are difficult to characterize. To complicate matters further, faint sources have larger positional uncertainties in the far-IR and hence have a higher possibility of a photometric mismatch.

In Figures 12 and 13 we compare our final sample of evolved stars to the entire HERITAGE BMC, the BMC candidate evolved stars which were identified as mismatch or probable YSOs and the BMC evolved star candidates confirmed spectroscopically as YSOs. As noted earlier, the spectroscopically confirmed sources are limited to the brightest stars in our sample due to signal-to-noise ratio constraints. In the SPIRE F_{250} and F_{350} CMD there is a considerable amount of overlap between the different populations, and the sources are primarily separated based on their brightness at 250 μm. Here we see a clear distinction between the bright spectroscopically confirmed YSOs and the evolved stars at $\log(F_{250})\sim2.7$, a similar cut is seen for the SMC despite its lower dust content which suggests a robust upper limit to the 250-micron flux of evolved stars.

The majority of the sources that we conclusively identify fall well above the completeness limit of the *Herschel* BMC. Although we detect a moderate number of faint evolved sources below this line we have invariably missed others; it is difficult to put a number on how may more of these faint sources might be evolved. The small spread in the F_{250}/F_{350} colour and the limited number of evolved stars detected in both bands prohibits the classification of sources using only their far-IR flux. If we are to clearly identify evolved sources additional mid-infrared data is required. Figure 13 shows a CMD which combines mid- and far-IR photometry; here the various classes of objects tend to occupy different regions of CMD space although we are not able to completely separate the two populations. Furthermore, by combining far-IR data with 8 μm photometry we effectively eliminate dust clumps and faint background galaxies from the CMD making it easier to distinguish the evolved sources.

5. Summary and conclusions

In this paper, we present a catalog of thirty five evolved stars and stellar end products which have been detected with PACS and SPIRE as part of the *Herschel* HERITAGE survey of the Magellanic Clouds. Our source identification method is based on mid-IR spectral confirmation, the SED characteristics, careful examination of the multi-wavelength images and includes constraints on the luminosity and comparisons with YSO models.

The sources detected in our catalog cover a wide range in luminosity and hence initial mass. We have identified thirteen low- to intermediate mass post main-sequence stars, which are either currently losing-mass at high rates or are evolved post-superwind objects. We find ten high mass stars, including four of the fifteen known B[e] stars in the Magellanic Clouds, and three extreme RSGs which are highly enshrouded by dust. Far-IR emission is also detected from the ejecta of SN1987A and from the supernova remnant N132D, both in the LMC. We have also identified far-IR emission from ten possible evolved star candidates.

This catalog lays the groundwork for future studies of the far-IR emission from evolved stars and stellar end products in the Magellanic Clouds. In a future paper we will provide in-depth treatment of the far-IR emission via radiative transfer modeling to determine if the emission originates from the circumstellar envelope, or if it is due to swept-up ISM dust.

We thank the referee Jacco van Loon for their

thorough and helpful comments. We acknowledge financial support from the NASA Herschel Science Center, JPL contracts # 1381522, # 1381650 & # 1350371. Jones and Meixner acknowledge support from NASA grant, NNX14AN06G, for this work. Sargent acknowledges support from NASA grant NNX13AD54G. This work is based on observations made with the *Herschel Space Observatory*, an ESA space observatory with science instruments provided by European-led Principal Investigator consortia and with important participation from NASA, and the *Spitzer* Space Telescope, which is operated by the Jet Propulsion Laboratory, California Institute of Technology under contract with NASA. This research relied on the following resources: NASA's Astrophysics Data System and the SIMBAD and VizieR databases, operated at the Centre de Données astronomiques de Strasbourg.

Facilities: *Herschel* (PACS, SPIRE) - European Space Agency's Herschel space observatory, *Spitzer* (IRS, IRAC, MIPS) - Spitzer Space Telescope satellite

REFERENCES

Aret, A., Kraus, M., Muratore, M. F., & Borges Fernandes, M. 2012, MNRAS, 423, 284

Barkat, Z., & Wheeler, J. C. 1988, ApJ, 332, 247

Barlow, M. J. 1987, MNRAS, 227, 161

Beelen, A., Cox, P., Benford, D. J., et al. 2006, ApJ, 642, 694

Bernard-Salas, J., Peeters, E., Sloan, G. C., et al. 2009, ApJ, 699, 1541

Bernard-Salas, J., Pottasch, S. R., Gutenkunst, S., Morris, P. W., & Houck, J. R. 2008, ApJ, 672, 274

Bertoldi, F., & Cox, P. 2002, A&A, 384, L11

Bica, E. L. D., Schmitt, H. R., Dutra, C. M., & Oliveira, H. L. 1999, AJ, 117, 238

Bjorkman, K. S., Miroshnichenko, A. S., Bjorkman, J. E., et al. 1998, ApJ, 509, 904

Blanco, V. M., Blanco, B. M., & McCarthy, M. F. 1980, ApJ, 242, 938

Blum, R. D., Mould, J. R., Olsen, K. A., et al. 2006, AJ, 132, 2034

Boffi, F. R., & Stanghellini, L. 1994, A&A, 284, 248

Bonanos, A. Z., Massa, D. L., Sewilo, M., et al. 2009, AJ, 138, 1003

Bonanos, A. Z., Lennon, D. J., Köhlinger, F., et al. 2010, AJ, 140, 416

Boroson, T. A., & Liebert, J. 1989, ApJ, 339, 844

Boyer, M. L., van Loon, J. T., McDonald, I., et al. 2010, ApJL, 711, L99

Boyer, M. L., Srinivasan, S., van Loon, J. T., et al. 2011, AJ, 142, 103

Boyer, M. L., Srinivasan, S., Riebel, D., et al. 2012, ApJ, 748, 40

Breysacher, J., Azzopardi, M., & Testor, G. 1999, A&AS, 137, 117

Buchanan, C. L., Kastner, J. H., Forrest, W. J., et al. 2006, AJ, 132, 1890

Cioni, M.-R. L., & Habing, H. J. 2003, A&A, 402, 133

Cox, N. L. J., Kerschbaum, F., van Marle, A.-J., et al. 2012, A&A, 537, A35

Crowther, P. A. 2007, ARA&A, 45, 177

Cutri, R. M., & 2MASS Team. 2004, in Bulletin of the American Astronomical Society, Vol. 36, American Astronomical Society Meeting Abstracts, 1487

de Grijp, M. H. K., Lub, J., & Miley, G. K. 1987, A&AS, 70, 95

Dijkstra, C., Waters, L. B. F. M., Kemper, F., et al. 2003, A&A, 399, 1037

Diolaiti, E., Bendinelli, O., Bonaccini, D., et al. 2000, in Society of Photo-Optical Instrumentation Engineers (SPIE) Conference Series, Vol. 4007, Adaptive Optical Systems Technology, ed. P. L. Wizinowich, 879–888

Dwek, E., Galliano, F., & Jones, A. P. 2007, ApJ, 662, 927

Egan, M. P., Van Dyk, S. D., & Price, S. D. 2001, AJ, 122, 1844

Elias, J. H., Frogel, J. A., & Schwering, P. B. W. 1986, ApJ, 302, 675

Fraser, O. J., Hawley, S. L., & Cook, K. H. 2008, AJ, 136, 1242

Gehrz, R. 1989, in IAU Symposium, Vol. 135, Interstellar Dust, ed. L. J. Allamandola & A. G. G. M. Tielens, 445

Gordon, K. D., Meixner, M., Meade, M. R., et al. 2011, AJ, 142, 102

Gouliermis, D., Kontizas, M., Kontizas, E., & Korakitis, R. 2003, A&A, 405, 111

Griffin, M. J., Abergel, A., Abreu, A., et al. 2010, A&A, 518, L3

Groenewegen, M. A. T., Waelkens, C., Barlow, M. J., et al. 2011, A&A, 526, A162

Gruendl, R. A., & Chu, Y.-H. 2009, ApJS, 184, 172

Gruendl, R. A., Chu, Y.-H., Seale, J. P., et al. 2008, ApJL, 688, L9

Guha Niyogi, S., Min, M., Meixner, M., et al. 2014, A&A, 569, A80

Harris, J., & Zaritsky, D. 2004, AJ, 127, 1531

Henize, K. G. 1956, ApJS, 2, 315

Herald, J. E., & Bianchi, L. 2007, ApJ, 661, 845

Heydari-Malayeri, M., & Melnick, J. 1992, A&A, 258, L13

Hora, J. L., Cohen, M., Ellis, R. G., et al. 2008, AJ, 135, 726

Humphreys, R. M., & Davidson, K. 1994, PASP, 106, 1025

Hutsemekers, D. 1994, A&A, 281, L81

Indebetouw, R., Matsuura, M., Dwek, E., et al. 2014, ApJL, 782, L2

Ita, Y., Onaka, T., Kato, D., et al. 2008, PASJ, 60, 435

Jones, A. P., Tielens, A. G. G. M., Hollenbach, D. J., & McKee, C. F. 1994, ApJ, 433, 797

Jones, O. C., Kemper, F., Srinivasan, S., et al. 2014, MNRAS, 440, 631

Jones, O. C., Kemper, F., Sargent, B. A., et al. 2012, MNRAS, 427, 3209

Joye, W. A., & Mandel, E. 2003, in Astronomical Society of the Pacific Conference Series, Vol. 295, Astronomical Data Analysis Software and Systems XII, ed. H. E. Payne, R. I. Jedrzejewski, & R. N. Hook, 489

Kastner, J. H., Buchanan, C., Sahai, R., Forrest, W. J., & Sargent, B. A. 2010, AJ, 139, 1993

Kastner, J. H., Buchanan, C. L., Sargent, B., & Forrest, W. J. 2006, ApJL, 638, L29

Kato, D., Nagashima, C., Nagayama, T., et al. 2007, PASJ, 59, 615

Keller, S. C., & Wood, P. R. 2006, ApJ, 642, 834

Kemper, F., Woods, P. M., Antoniou, V., et al. 2010, PASP, 122, 683

Kerschbaum, F., Ladjal, D., Ottensamer, R., et al. 2010, A&A, 518, L140

Kim, S., Kwon, E., Madden, S. C., et al. 2010, A&A, 518, L75

Kozłowski, S., & Kochanek, C. S. 2009, ApJ, 701, 508

Kraus, M., Borges Fernandes, M., & de Araújo, F. X. 2007, A&A, 463, 627

Lakićević, M., van Loon, J. T., Meixner, M., et al. 2015, ApJ, 799, 50

Lamers, H. J. G. L. M., Bastiaanse, M. V., Aerts, C., & Spoon, H. W. W. 1998, A&A, 335, 605

Lennon, D. J., Wobig, D., Kudritzki, R.-P., & Stahl, O. 1993, Space Sci. Rev., 66, 207

Levesque, E. M., Massey, P., Olsen, K. A. G., & Plez, B. 2007, ApJ, 667, 202

Lindsay, E. M. 1961, AJ, 66, 169

Maercker, M., Mohamed, S., Vlemmings, W. H. T., et al. 2012, Nature, 490, 232

Marshall, J. R., van Loon, J. T., Matsuura, M., et al. 2004, MNRAS, 355, 1348

Massey, P. 2002, ApJS, 141, 81

Massey, P., & Olsen, K. A. G. 2003, AJ, 126, 2867

Matsuura, M., Barlow, M. J., Zijlstra, A. A., et al. 2009, MNRAS, 396, 918

Matsuura, M., Dwek, E., Meixner, M., et al. 2011, Science, 333, 1258

Matsuura, M., Bernard-Salas, J., Lloyd Evans, T., et al. 2014, MNRAS, 439, 1472

Matsuura, M., Dwek, E., Barlow, M. J., et al. 2015, ApJ, 800, 50

Meixner, M., Gordon, K. D., Indebetouw, R., et al. 2006, AJ, 132, 2268

Meixner, M., Hony, S., Madden, S., et al. 2010, in Bulletin of the American Astronomical Society, Vol. 42, American Astronomical Society Meeting Abstracts 215, 459.22

Meixner, M., Panuzzo, P., Roman-Duval, J., et al. 2013, AJ, 146, 62

Mennickent, R. E., Pietrzyński, G., Gieren, W., & Szewczyk, O. 2002, A&A, 393, 887

Meynadier, F., & Heydari-Malayeri, M. 2007, A&A, 461, 565

Meyssonnier, N., & Azzopardi, M. 1993, A&AS, 102, 451

Michałowski, M. J., Murphy, E. J., Hjorth, J., et al. 2010, A&A, 522, A15

Moffat, A. F. J. 1991, A&A, 244, L9

Morse, J. A., Winkler, P. F., & Kirshner, R. P. 1995, AJ, 109, 2104

Murphy, M. T., & Bessell, M. S. 2000, MNRAS, 311, 741

Ngeow, C., & Kanbur, S. M. 2008, ApJ, 679, 76

Ohnaka, K., Driebe, T., Hofmann, K.-H., Weigelt, G., & Wittkowski, M. 2008, A&A, 484, 371

Oliveira, J. M., van Loon, J. T., Chen, C.-H. R., et al. 2009, ApJ, 707, 1269

Oliveira, J. M., van Loon, J. T., Sloan, G. C., et al. 2013, MNRAS, 428, 3001

Otsuka, M., van Loon, J. T., Long, K. S., et al. 2010, A&A, 518, L139

Pilbratt, G. 2010, in Bulletin of the American Astronomical Society, Vol. 41, Bulletin of the American Astronomical Society, 418

Poglitsch, A., Waelkens, C., Geis, N., et al. 2010, A&A, 518, L2

Porter, J. M. 2003, A&A, 398, 631

Reid, W. A., & Parker, Q. A. 2006, MNRAS, 373, 521

—. 2012, MNRAS, 425, 355

Rho, J., Reach, W. T., Tappe, A., et al. 2009, ApJ, 700, 579

Riebel, D., Srinivasan, S., Sargent, B., & Meixner, M. 2012, ApJ, 753, 71

Robitaille, T. P., Whitney, B. A., Indebetouw, R., & Wood, K. 2007, ApJS, 169, 328

Robitaille, T. P., Whitney, B. A., Indebetouw, R., Wood, K., & Denzmore, P. 2006, ApJS, 167, 256

Roche, P. F., Aitken, D. K., & Smith, C. H. 1993, MNRAS, 262, 301

Ruffle, P. M. E., Kemper, F., Jones, O. C., et al. 2015, MNRAS, 451, 3504

Russell, S. C., & Dopita, M. A. 1992, ApJ, 384, 508

Samus, N. N., Durlevich, O. V., & et al. 2004, VizieR Online Data Catalog, 2250, 0

Schlegel, D. J., Finkbeiner, D. P., & Davis, M. 1998, ApJ, 500, 525

Seale, J. P., Meixner, M., Sewiło, M., et al. 2014, AJ, 148, 124

Sewiło, M., Carlson, L. R., Seale, J. P., et al. 2013, ApJ, 778, 15

Shaw, R. A., Stanghellini, L., Mutchler, M., Balick, B., & Blades, J. C. 2001, ApJ, 548, 727

Shaw, R. A., Stanghellini, L., Villaver, E., & Mutchler, M. 2006, ApJS, 167, 201

Sheets, H. A., Bolatto, A. D., van Loon, J. T., et al. 2013, ApJ, 771, 111

Skrutskie, M. F., Cutri, R. M., Stiening, R., et al. 2006, AJ, 131, 1163

Sloan, G. C., Lagadec, E., Zijlstra, A. A., et al. 2014, ApJ, 791, 28

Smith, R. C., & MCELS Team. 1998, PASA, 15, 163

Srinivasan, S., Meixner, M., Leitherer, C., et al. 2009, AJ, 137, 4810

Stahl, O., Wolf, B., Klare, G., et al. 1983, A&A, 127, 49

Stanghellini, L., Blades, J. C., Osmer, S. J., Barlow, M. J., & Liu, X.-W. 1999, ApJ, 510, 687

Stanghellini, L., García-Lario, P., García-Hernández, D. A., et al. 2007, ApJ, 671, 1669

Stanghellini, L., Shaw, R. A., Balick, B., et al. 2003, ApJ, 596, 997

Stanghellini, L., Shaw, R. A., & Gilmore, D. 2005, ApJ, 622, 294

Szczygieł, D. M., Stanek, K. Z., Bonanos, A. Z., et al. 2010, AJ, 140, 14

Szewczyk, O., Pietrzyński, G., Gieren, W., et al. 2009, AJ, 138, 1661

Tappe, A., Rho, J., & Reach, W. T. 2006, ApJ, 653, 267

Tchernyshyov, K., Meixner, M., Seale, J., et al. 2015, ArXiv e-prints, arXiv:1503.08852

Temim, T., Dwek, E., Tchernyshyov, K., et al. 2015, ApJ, 799, 158

Testor, G., Heydari-Malayeri, M., Chen, C.-H. R., et al. 2014, A&A, 564, A31

Trams, N. R., van Loon, J. T., Waters, L. B. F. M., et al. 1999, A&A, 346, 843

van Aarle, E., van Winckel, H., Lloyd Evans, T., et al. 2011, A&A, 530, A90

van der Marel, R. P., & Cioni, M.-R. L. 2001, AJ, 122, 1807

van Loon, J. T., Cioni, M., Zijlstra, A. A., & Loup, C. 2005a, A&A, 438, 273

van Loon, J. T., Hekkert, P. T. L., Bujarrabal, V., Zijlstra, A. A., & Nyman, L.-Å. 1998, A&A, 337, 141

van Loon, J. T., Marshall, J. R., & Zijlstra, A. A. 2005b, A&A, 442, 597

van Loon, J. T., Oliveira, J. M., Gordon, K. D., Sloan, G. C., & Engelbracht, C. W. 2010a, AJ, 139, 1553

van Loon, J. T., Zijlstra, A. A., Bujarrabal, V., & Nyman, L.-Å. 1996, A&A, 306, L29

—. 2001, A&A, 368, 950

van Loon, J. T., Zijlstra, A. A., Whitelock, P. A., et al. 1997, A&A, 325, 585

van Loon, J. T., Oliveira, J. M., Gordon, K. D., et al. 2010b, AJ, 139, 68

Villaver, E., Stanghellini, L., & Shaw, R. A. 2003, ApJ, 597, 298

Volk, K., Hrivnak, B. J., Matsuura, M., et al. 2011, ApJ, 735, 127

Voors, R. H. M., Waters, L. B. F. M., Morris, P. W., et al. 1999, A&A, 341, L67

Whitney, B. A., Sewilo, M., Indebetouw, R., et al. 2008, AJ, 136, 18

Williams, B. J., Borkowski, K. J., Reynolds, S. P., et al. 2006, ApJL, 652, L33

Wood, P. R., Bessell, M. S., & Fox, M. W. 1983, ApJ, 272, 99

Wood, P. R., Bessell, M. S., & Whiteoak, J. B. 1986, ApJL, 306, L81

Wood, P. R., Meatheringham, S. J., Dopita, M. A., & Morgan, D. H. 1987, ApJ, 320, 178

Wood, P. R., Whiteoak, J. B., Hughes, S. M. G., et al. 1992, ApJ, 397, 552

Wooden, D. H., Rank, D. M., Bregman, J. D., et al. 1993, ApJS, 88, 477

Woods, P. M., Oliveira, J. M., Kemper, F., et al. 2011, MNRAS, 411, 1597

Wright, E. L., Eisenhardt, P. R. M., Mainzer, A. K., et al. 2010, AJ, 140, 1868

Zaritsky, D., Harris, J., & Thompson, I. 1997, AJ, 114, 1002

Zickgraf, F.-J., Wolf, B., Leitherer, C., Appenzeller, I., & Stahl, O. 1986, A&A, 163, 119

Zickgraf, F.-J., Wolf, B., Stahl, O., Leitherer, C., & Klare, G. 1985, A&A, 143, 421

This 2-column preprint was prepared with the AAS LaTeX macros v5.2.